Doctoral Dissertation
Academic Year 2023

Applications of Metabolomics and Proteomics to Study the Biological Effects of Drugs

Graduate School of Media and Governance
Keio University
Guo Jing

Applications of metabolomics and proteomics to study the biological effects of drugs

Abstract

Metabolomics and proteomics is a rapidly advancing area of research. Metabolites and proteins are functional and signaling molecules that often represent biological phenotypes and states. In recent years, mass spectrometry (MS) has gained widespread use in metabolomics and proteomics to monitor intracellular changes in cells, and by comprehensively measuring changes in these research objects it is possible to understand and elucidate the mechanisms that lead to different phenotypes. In Chapter 2, we identified the charged metabolites of 30 different types of Chinese herbal extracts and used metabolomics to investigate and explain the “cold and hot natured” of the traditional Chinese herbal classification. Chapter 3 focuses on the metabolomic analysis of normal and cisplatin (CDDP)-resistant cell lines to address the issue of chemotherapy resistance in ovarian cancer. The study revealed that CDDP-resistant cells exhibited significantly elevated levels of glutamine, and inhibiting glutamine metabolism led to reduced glutathione levels and decreased CDDP resistance. Additionally, the study found that the expression of glutamine synthetase (GS) was nearly suppressed in resistant cells, and knockdown of GS in normal ovarian cancer cells increased their CDDP resistance. Therefore, Chapter 4 investigated GS and its potential functionality in three different cultured cell lines (from ovarian and lung cancer) using omics approaches. Although GS expression varied among the three cell lines, knockdown of GS resulted in decreased platinum drug resistance. Proteomics research indicated that GS downregulation significantly decreased ferrochelatase, the terminal enzyme in the heme biosynthesis pathway, in the three cell lines, suggesting increased protoporphyrin and decreased heme synthesis. Moreover, GS downregulation activated the NF-κB pathway, an immune response pathway, while inhibiting cell responses to drugs. In summary, this research has provided novel insights into the effects of herbal medicines and anticancer drugs through metabolomics and proteomics using mass spectrometry.

Keyword: CE-MS, cancer, traditional Chinese medicine, drug resistance, glutamate synthetase

メタボロミクス・プロテオミクスによる薬剤の生体への作用解析

要旨

メタボロミクスとプロテオミクスは急速に進化している研究分野であり、広範囲な視点から生物学を理解する可能性を提供する。代謝産物とタンパク質は生物の表現型や状態を反映すると考えられ、生体内の機能性分子およびシグナル伝達分子の役割を担う。近年、メタボロミクスやプロテオミクスでは、細胞内の分子の変動をモニターするために質量分析技術が広く使われ、このような測定対象物質の変化を網羅的に測定することで、様々な表現型を生み出す機序を解明することができる。第 2 章では、30 種類の生薬抽出物のイオン性代謝産物を調べ、メタボロミクスの観点から中国伝統医学の分類法の“寒性と熱性”を解析した。第 3 章では、卵巣がんの化学療法抵抗性の問題に取り組み、正常卵巣癌細胞と抗がん剤であるシスプラチンの耐性を獲得した卵巣癌細胞のメタボローム解析を行った。その結果、耐性細胞のグルタミン量は極めて高いことが判明した。そこで、グルタミン代謝を阻害することによりグルタチオン量を減少させ、シスプラチン耐性を低下されることを見いだした。また、シスプラチン耐性細胞ではグルタミン合成酵素 (GS) の発現がほぼ抑制されており、正常卵巣がん細胞で GS をノックダウンするとシスプラチン耐性が高まることがわかった。そこで、第 4 章では GS に着目し、オミックスアプローチを用いて 3 種類の培養細胞株（卵巣がん、肺がん由来）において、その機能を検討した。GS は 3 つの細胞株での発現量が異なるにもかかわらず、GS のノックダウンはプラチナ製剤耐性を低下させた。プロテオミクス解析の結果、GS のダウンレギュレーションは、3 つの細胞株でヘム生合成経路の最後の反応酵素であるフェロケラターゼの低下およびその上流の酵素の上昇がみられ、プロトポルフィリの増加とヘム合成の減少が示唆された。また、GS のダウンレギュレーションは、免疫応答経路である NF-κB 経路を活性化し、薬剤に対する細胞の応答を阻害することが判明した。まとめると、今回の研究によって、質量分析計を用いたメタボロミクスやプロテオミクスにより、漢方薬や抗がん剤が生体に示す作用を新たに見出すことができた。

キーワード： CE-MS, 癌, 漢方薬, 薬剤耐性, グルタミン合成酵素

Table of Contents

List of Figures

List of Tables

Chapter 1 Introduction

1.1 The Importance of Omics in Scientific Method

Omics is an analytical methodology based on big data. In traditional scientific methodology, observations are made, and questions are raised, followed by the creation of a hypothesis and its verifiable explanation. Thereafter, experiments are performed to validate the theory. Finally, depending on the obtained results, responses are given or new hypotheses are presented. However, in the traditional methodology, the hypothesis construction step is considerably dependent on previous experience. Therefore, biased observations of new things can lead to "the blind men and an elephant" misconceptions. This embarrassment can be efficiently avoided with the utilization of big data and omics methods. Researchers can select factors via omics data analysis and then experimentally validate their selections based on the obtained results[1]. Moreover, individual differences influence judgment in biology; the omics approach can increase the universality and reproducibility of results.

Based on the objectives of the analysis, omics are classified into genomics, transcriptomics, proteomics, and metabolomics. Genes are employed as the fundamental blueprints when cells produce materials such as proteins. Specific sections of genes are transcribed (transcript) to synthesize mRNA when the genetic information is utilized. The overall quantity of mRNA information in an organism is referred to as the transcriptome. Proteins are synthesized based on the mRNA information, and the total amount of proteins in an organism is referred to as the proteome. Cells metabolize and produce metabolites from these various materials, resulting in trait manifestations such as variances in hair or eye color (phenotype) [2].

Current research methods in genomics depend on next-generation sequencing to fragment the genome followed by de novo assembly method or iterative assembly and subsequent data analysis such as gene annotation[3]. Transcriptomics is the study of the sum of mRNA at a given point in time, and it routinely employs microarray or sequencing technologies. Microarray work with known gene probes, and RNA-seq has the potential to discover new mRNA[4]. Proteomics identified proteins mostly using

2D-gel electrophoresis until the twenty-first century, but currently, mass spectrometry (MS) is primarily used[5]. The principle is similar to that of genomics, in which proteases are cleaved into peptides, the protein sequence is inferred by mass inversion, and finally, the known and unknown protein sequences are identified by a deep search. Metabolomic analysis of metabolites, which contain molecules such as nucleotides, amino acids, sugars, organic acids, and lipids, is also performed mainly by liquid chromatography and MS. In conclusion, all the aforementioned techniques search for variables globally and are top-down research approaches.

1.2 Significance of metabolomics in pharmacy

Metabolites are the most effective molecules to reflect biological phenotype and state[6]. These molecules being the end products of cellular regulatory processes can be regarded as the ultimate response of biological systems to control genetic or environmental changes. This implies, if properly interpreted, metabolomics can provide information about a cascade of changes at the DNA, RNA and protein levels. In some cases, this method may be the most sensitive way to identify pathological variants, because even small changes in protein expression or structure can result in significant changes in protein activity and metabolite levels[7].

In practice, metabolomics is defined as the analysis of small-molecule metabolites (≤1500 daltons and non-peptides) in biological samples[7]. Advances in MS have considerably improved the efficiency of metabolomics, which can simultaneous identification of hundreds to thousands of molecules. Therefore, MS is currently an ideal tool for the application of metabolomics. Moreover, with the development of MS instruments and methods, more accurate detection can be performed, and the detection speed and flux are improving. MS-based metabolomics demonstrates several applications in drug discovery and development[8]. For example, mass spectroscopy significantly contributes to the enhanced understanding of the role of candidate drugs and improves their targeting capabilities or comprehensive non-invasive analysis of metabolic biomarkers for early disease detection and identification of residual disease after surgery. Therefore, mass spectroscopy has become an indispensable tool in combined clinical monitoring and drug development.

Cancer is one of the most challenging problems in modern medicine. Unlike bacterial or viral infections, cancer cells are derived from the own body cells of the affected individual. Therefore, these cells are very similar in composition to the normal cells in the body. In addition, considerable variations in developmental states (different stages of cancer development or drug resistance) are observed. Hence, drugs that selectively work on cancer cells without harming normal cells or that work at all stages of cancer development are essential for cancer therapy. Based on the development of metabolomics technology, currently, researchers have concluded that metabolic reprogramming is a cancer marker[9]. In recent years, increasing evidence has been available that suggests reprogrammed cellular metabolism supports tumor initiation, progression, metastasis, and drug resistance[9,10]. By performing qualitative and quantitative analyses of small molecules within cells or tissues, metabolomics provides static data at specific time points, while metabolic flow analyses can use stable isotopes; therefore, metabolic turnover was explored dynamically[11,12]. Thus, metabolomics can be used to understand the metabolic imbalance in cancer cells, determine therapeutic targets, and facilitate drug development for cancer therapy. Therapeutic strategies that involve target metabolic enzymes have achieved several breakthroughs, and currently, dozens of small-molecule inhibitors targeting more than a dozen metabolic enzymes are under preclinical and clinical investigations[13]. This strategy alters those activities of metabolic enzymes which are necessary for the cancer cells to maintain growth (often referred to as metabolic dependence), but the host metabolism can tolerate the inhibition of this activity. Therefore, highly specific and preferentially isoenzyme-selective metabolic inhibitors are critical to the safety and efficacy of the developed drug.

Plants have been a source of numerous drugs used in modern therapies, particularly in the treatment of cancer, with more than 50% of the anticancer drugs initially derived from natural products[14,15]. Regarding the application of plants in pharmacy, traditional Chinese medicine (TCM) is worth mentioning. Unlike Western medicine represented by Ancient Greek Traditional Medicine, which pays more attention to the human body itself, Eastern Traditional Medicine, such as TCM and Indian Traditional Medicine, focuses on aspects such as the use of plants and treating diseases with minerals. TCM is usually a mixture of several plants. It had been developed and practiced for thousands of years before the advent of modern medicine and developed complex theories that were

handed down by books[16]. Because these theories are based on philosophy and clinical experience, they lack modern scientific support and molecular basis, and mechanistic understanding. Therefore, the quality control of traditional drugs, their clinical efficacy, and the investigation of molecular mechanisms are imminent[17]. With the increasing maturity of metabolomics techniques, the use of metabolomics to study TCM began to increase gradually[18]. However, because of the complex chemical composition of TCM, thousands of compounds can be produced by just one medicinal plant, and several of them simultaneously interact with different disease targets[19,20]. Therefore, effective identification of the functional compounds and deciphering their pharmacological effects is a challenge to the scientific development of Chinese pharmacy[21,22]. On the one hand, metabolomics technology can provide a high-performance analytical method to characterize the medicinal plant compound (primary and secondary metabolites), which is more conducive to the standardization of medicinal plant quality. On the other hand, metabolomics significantly contributes to understanding the effects of medicinal plants on the metabolic function in humans or model animals to unravel pharmacological efficacy and therapeutic mechanisms[23-26].

1.3 Significance of proteomics in pharmacy

In the era of functional genomics, proteomics is a discipline that studies the composition, activity, and interaction of proteins in cells as a whole. Most research to date has concentrated on RNA detection. However, because proteins are found downstream of transcription and are directly involved in crucial physiological processes, typically show an insignificant relationship exists between the protein levels and transcript levels[27]. In the Human Protein Atlas Project, although The Human proteome Atlas is mapped based on the transcriptome data and antibody staining, as well as the RNA-based classification of tissue-specific expression, the issues of precise quantification and antibody specificity still exist[28]. Currently, MS-based proteomics quantifies human proteins, accounting for more than 90% of the protein species encoded by the genes[29,30]. Moreover, the most advanced proteomic technology enables highly reliable in-depth analysis of cancer proteome to realize clinical molecular typing and discover new target molecules, driving the development of precision medicine[31,32].

Proteomics is preclinically employed for target recognition and characterization, candidate drug selection and characterization, and clinically for biomarker discovery and the development of novel anticancer medicines[33,34]. In addition, proteomics can be used to analyze biological components, secreted proteins, protein translational modifications and protein-protein interaction networks by using specific procedures[35]. More precise biomarker targets can be found and created for diagnosis and treatment by mapping altered signaling pathways and finding altered protein expression that causes carcinogenesis, invasion, and metastasis. Taken together, the discovery of biomarkers by proteomics holds great promise for identifying novel intracellular signaling pathways that could lead to the discovery of new therapeutic targets, as well as facilitating the understanding of important pathway regulators and biomarkers.

1.4 Application of MS-based metabolomics and proteomics analyses

Three initiatives in this thesis make use of the metabolomics and proteomics research methodologies.

In Chapter 2, the project aimed to analyze the metabolites of several Chinese herbal medicines by CE-MS. CE-MS is mainly used for polar molecules. In a few cases have been utilized to test for Chinese herbal medicines, but it has the advantages of high resolution, low sample and solvent consumption, quick analysis times, and high separation efficiencies[36]. Although the study of “cold and hot” is the dominant core in the theoretical research of TCM, some articles speculate that the content of some metabolites may be related to cold and hot, though the distinction has never been clearly explained by modern science[37]. Moreover, the study analyzed the relationship between their molecular similarity and "cold and hot".

In Chapter 3, cancer cells were studied by metabolomic analysis of ovarian cancer cell lines and their cisplatin (CDDP)-resistant cell lines using CE-MS and metabolic flux techniques. It was found that there were significant differences in glutamine metabolism between the two cell lines. Metabolic flux analysis using stable isotope glutamine revealed differences in the regulation of energy metabolism and changes in GS by L-glutamine in the tolerant cell lines. The analysis also showed that GS regulation could effectively control CDDP-induced drug resistance.

In Chapter 4, the study follows up on the previous chapter, which focused on the function of GS. GS knockdown in a variety of cell lines by recombinant lentiviral infection suggested that GS could increase the platinum-based drugs resistance of tumor cells. The GS knockdown strain and the control group were compared using the metabolic flux technique of CE-MS and the proteomic technique of LC-MS/MS. It was found to trigger the activation of several pathways that maintain the proliferation and survival of tumor cells.

Chapter 2 Quantitative and molecular similarity analyses of the metabolites of cold- and hot-natured Chinese herbs

2.1 Introduction

In recent years, TCM has gained recognition worldwide as a valuable treatment for chronic and complex diseases. The World Health Organization has estimated that over 80% of the world's population relies on herbal medicines[38]. With centuries of clinical practice and development, recent endeavors have focused on scientific studies to establish the principles of TCM. However, ancient books on TCM generally present experience-based principles, obscuring the details needed for diagnosing and prescribing proper herbs for disease treatment. Therefore, it is important to clearly understand the nature of herbal medicines and illustrate their therapeutic uses in detail so as to provide a comprehensive guide to TCM inheritance because it is a treasure house for humans.

TCM recipes use herbs alone or in a mixture. Based on a patient's condition, a recipe is written for effective treatment using adjusted amounts or a combination of various ingredients by adding or deleting individual herbs. According to the therapeutic properties described in ancient books, such as *Shennong Ben Cao Jing* and *Compendium of Bencao*, Chinese herbs represent complementary forces of "four natures and five flavors." For rebalancing the Yin and Yang of the body, Chinese herbs can be classified into four groups: warm, hot, cold, and cool; these are the so-called four natures, also known as the four properties. In clinical application, the principal of healing in TCM is to balance the disturbed Yin–Yang in the body using appropriate therapy to restore the harmony of the entire body. To this end, hot-natured herbs are used for treating cold syndromes and cold-natured herbs are used for treating hot syndromes. Although the four natures of Chinese herbs have been widely known by our

ancestors for more than 2,000 years, the scientific basis of their classification remains unclear[39].

Among the TCM substances (botanical, animal, and mineral), more than 90% are of botanical origin, and the roots, stems, flowers, and fruits are medicinally useful[40]. Recent studies have proven the effects of the combination of herbal medicines[41,42]. Recently, coupled with statistical analysis, cold- and hot-natured Chinese herbs were investigated by using the state-of-the-art analytical techniques for the determination of amino acids and lipids[37]. The application of metabolomics analysis and multivariate data analysis to herbal medicine is also gaining increased attention[26,43-45]. Gas chromatography–MS (GC–MS), liquid chromatography–MS (LC–MS), and nuclear magnetic resonance are used for the analysis of TCMs[46,47].

Capillary electrophoresis–time-of-flight MS (CE–TOF/MS) is an analytical technique used to qualitatively and quantitatively detect small-molecule compounds and is particularly well-suited for the detection of charged compounds in organisms[48,49]. This technique has been broadly applied in biological samples, such as plants, and herbal preparations[44,50]. When analyzing herbal species, providing a comprehensive evaluation for all metabolites remains a technical challenge[24].

In this study, 30 representative cold- and hot-natured herbs were selected for comparative analysis of the contents of charged small molecules in metabolites. Our study focused on the active ingredients, including alkaloids, organic acids, amino acids, flavonoids, and small-molecule polyphenols, that act on the human body[51]. Based on the identification results, the hot and cold natured of the compounds in Chinese herbs were characterized. These results may help elucidate the holistic molecular mechanisms underlying the determination of the intrinsic hot or cold nature of Chinese herbs.

2.2 Materials and methods

2.2.1 Herbal medicine preparation

A total of 30 Chinese herbs were selected (Table2-1), of which 15 were cold-natured and 15 were hot-nature herbs according to the description of the Chinese Pharmacopoeia (V.2015). These herbs were purchased from Beijing Tong Ren Tang

Group Co. Ltd. (Beijing, China). Researchers have analyzed the relationship between the four natures of herbal medicine and plant families[52]. However, the selection of herbs in our study was only based on only the four natures rather than on the plant family. Plant families with both hot/warm and cold natured, including Rutaceae, Asteraceae, and Ranunculaceae, were also present in the 30 chosen herbs.

The preparation of herbs referred to the previous study[50]. In brief, 100 mg of each sample was frozen in liquid nitrogen and then homogenized into a single powder using a shocker (TOMY MS-100R) at 1,500 rpm for 180 × 2 s. After the preliminary treatment, the samples were processed by adding 1,250 μL of 60% ethanol solution containing 8 μM internal standard 1 (containing l-methionine sulfone, 2-morpholinoethanesulfonic acid, and D-Camphor-10-sulfonic acid) and extracting the samples for 2 h. The supernatants were collected via centrifugation to obtain the extracted ingredients. The pellets containing plant residues, polysaccharides, and proteins were removed. The supernatants were transferred into 500-Da centrifugal filter tubes and recentrifuged at 9,100 ×g and at 4°C for 3 h, followed by filtering the samples. After filtration, the liquid samples were placed in a vacuum dryer (35°C, 3 h) for drying. The dried samples were forcefully dissolved with 200 μM Milli-Q water containing internal standard 2 (containing 3-aminopyrrolidine and trimesate) using a vortex.

Table2-1 Names and properties of the 30 Chinese herbs used for metabolite extraction

Number	Name	Latin index	Familia	Medicinal part	Natures	Flavor
1	Radix Aconiti Praeparata	*Aconitum carmichaelii* Debeaux	Ranunculaceae	Root	Hot	Pungent, Sweet
2	Cortex Cinnamomi	*Cinnamomum cassia* Nees ex Blume	Lauraceae	Bark	Hot	Pungent, Sweet
3	Rhizoma Zingiberis	*Zingiber officinale* Rosc.	Zingiberaceae	Rhizome	Hot	Pungent
4	Rhizoma alpiniae officinarum	*Alpinia officinarum* Hance	Zingiberaceae	Rhizome	Hot	Pungent
5	Fructus foeniculi	*Foeniculum vulgare* Mill.	Umbelliferae	Fruit	Warm	Pungent

Number	Name	Latin index	Familia	Medicinal part	Natures	Flavor
6	Flos caryophylli	*Syzygium aromaticum (L.)* Merr. & L.M.Perry	Myrtaceae	Flower bud	Warm	Pungent
7	Pericarpium zanthoxyli	*Zanthoxylum bungeanum* Maxim.	Rutaceae	Pericarp	Warm	Pungent
8	Pericarpium citri reticulatae	*Citrus reticulata* Blanco	Rutaceae	Pericarp	Warm	Pungent, Bitter
9	Pericarpium citri reticulatae viride	*Citrus reticulata* Blanco	Rutaceae	Pericarp	Warm	Pungent, Bitter
10	Fructus aurantii immaturus	*Citrus × aurantium* Linn.	Rutaceae	Fruit	Warm	Pungent, Bitter
11	Radix aucklandiae	*Aucklandia lappa* DC.	Asteraceae	Root	Warm	Pungent, Bitter
12	Radix linderae	*Lindera aggregata (Sims)* Kosterm.	Lauraceae	Root	Warm	Pungent
13	Fructus citri sarcodactylis	*Citrus medica var. sarcodactylis (Noot.)* Swingle	Rutaceae	Fruit	Warm	Pungent, Bitter
14	Rhizoma chuanxiong	*Ligusticum sinense 'Chuanxiong'* S. H. Qiu et al.	Umbelliferae	Rhizome	Warm	Pungent
15	Semen arecae	*Areca catechu* Linn.	Palmae	Seed	Warm	Pungent, Bitter
16	Bulbus fritillariae cirrhosae	*Fritillaria cirrhosa D.* Don	Liliaceae	Rhizome	Cold	Bitter, Sweet
17	Radix scutellariae	*Scutellaria baicalensis* Georgi	Labiatae	Root	Cold	Bitter
18	Cortex phellodendri	*Phellodendron chinense* Schneid.	Rutaceae	Bark	Cold	Bitter
19	Radix gentianae	*Gentiana scabra* Bunge	Gentianaceae	Rhizome	Cold	Bitter
20	Radix sophorae flavescentis	*Sophora flavescens Ait.*	Papilionaceae	Root	Cold	Bitter

Number	Name	Latin index	Familia	Medicinal part	Natures	Flavor
21	Cortex fraxini	*Fraxinus chinensis subsp. rhynchophylla (Hance) E.* Murray	Oleaceae	Bark	Cold	Bitter
22	Cortex dictamni	*Dictamnus dasycarpus* Turcz.	Rutaceae	Velamen	Cold	Bitter
23	Folium isatidis	*Isatis tinctoria* Linn.	Cruciferae	Leaf	Cold	Bitter
24	Radix isatidis	*Isatis tinctoria* Linn.	Cruciferae	Root	Cold	Bitter
25	Herba andrographis	*Andrographis paniculata (Burm. f.)* Nees	Acanthaceae	Stem leaf	Cold	Bitter
26	Radix sophorae tonkinensis	*Euchresta japonica* Regel	Papilionaceae	Rhizome	Cold	Bitter
27	Herba artemisiae annuae	*Artemisia annua* L.	Compositae	Stem leaf	Cold	Bitter, Pungent
28	Radix et rhizoma rhei	*Rheum palmatum* Linn	Polygonaceae	Rhizome	Cold	Bitter
29	Rhizoma belamcandae	*Belamcanda chinensis (Linn.)* DC.	Iridaceae	Rhizome	Cold	Bitter
30	Radix Pulsatillae	*Pulsatilla chinensis (Bunge)* Regel	Ranunculaceae	Root	Cold	Bitter

2.2.2 Measurement conditions for CE–TOF/MS

The instrumentation and measurement conditions used for CE–TOF/MS were as described elsewhere[49,53]. In the positive ion mode, samples were separated in a fused silca capillary (50 μm i.d. × 100 cm) using 1 M formic acid as the electrophoretic and equilibrium buffer. Samples were injected under a pressure of 50 mbar for 3 s (approximately 3 μL) at an applied voltage of +30 kV. During the analysis, 50% (v/v) methanol containing 5 mM ammonium acetate and 0.5 M reserpin was used as the sheath liquid at a flow rate of 10 μL/min. In the negative ion mode, separation was

performed on a capillary SMILE (+) (Nacalai Tesque, Kyoto, Japan) using 50 mM ammonium acetate (pH 8.5) as the mobile phase. Samples were injected under a pressure of 50 mbar for 30 s at an applied voltage of −30 kV.

2.2.3 Data processing

The data measured via CE–TOF/MS were perprocessed using the MasterHands ver.2 software[54]. Noise-filtering, baseline correction, peak detection, and peak area integration were performed on mass/charge ratio (m/z) 0.02–width sliced electropherograms. The migration time was normalized using dynamic programming and simplex optimization. Peaks with small differences in their m/z values (<20 ppm) and normalized migration times (<1.0 min) were treated as features. External standards based on m/z values and migration times were used for identification and concentration calibration. To determine the concentrations of the compounds, the integral value (area) of the peak area, area of the sample compound, and area of the relative internal and external standards were calculated.

2.2.4 Statistical analysis

1) Discriminant analysis

The concentration of each metabolite was represented as the average of three samples. The differences in metabolites between the two independent groups, i.e., cold- and hot-natured groups, were detected using the Mann–Whitney U test using the MeV TM4 software (Dana-Farber Cancer Institute, Boston, MA)[55].

2) Principal components analysis (PCA)

PCA as an exploratory tool for data analysis used variables from a variety of components as a set of summary indices to observe the changing trend of all data. Analysis was conducted using the statistical software JMP ver.10 (SAS Institute Inc., Cary, NC, USA).

3) Molecular fingerprints and similarity searching

The commonly used algorithm to calculate the similarity of the compounds is the Tanimoto coefficient. Depending on the source of the structural information of the molecule provided by the public database of PubChem Compound, the structure data

files of the identified metabolites were used for analysis[56]. The Tanimoto coefficient is an index to calculate the degree of similarity of two clusters using similarity calculation (Equation 1) by comparing their molecular fingerprints in chemical systems[57]. In Equation 1, A and B are represented by vectors calculated from the local structures of various substances. When vectors A and Vector B are exactly equal 1, it is not at all equal to 0. For this reason, the closer the value is to 1, the higher is the similarity. The software Open Babel 2.3.0 was used to calculate the Tanimoto coefficients of all molecules[58].

$$T(A,B) = \frac{|\mathrm{A} \cap \mathrm{B}|}{|\mathrm{A}| + |\mathrm{B}| - |\mathrm{A} \cap \mathrm{B}|} \qquad (1)$$

4) Molecule cluster analysis

Molecule cluster analysis is a hierarchical clustering approach to discover the relationship between data by calculating the distance between the compounds extracted from the herbs and molecule cluster. In each of the succeeding steps, the closest clusters were merged to obtain a hierarchical structure. The Tanimoto coefficient was calculated based on the similarity between the substances. Molecule cluster analysis was performed using the Mev TM4 V4.6 analysis software[59] based on Spearman correlation coefficient (nonparametric method) and was classified based on average index.

2.3 Results

2.3.1 Profiling of the charged metabolites in TCMs

CE–TOF/MS-based metabolomics analysis was performed to detect the metabolites, including amino acids, organic acids, alkaloids, and nucleotides, in Chinese herbs. In total, 416 charged small molecules matched with the compounds in our standard library. Notably, despite a clear difference in metabolites between different herbs, there was a general metabolite-by-metabolite similarity among the herbs, and 193 identical metabolites were detected in most herbs. In the present study, to accelerate the similarity search, the lead 193 metabolites identified from over 16 herbs were screened using metabolomics for cluster analysis. The heatmap clusters based on the metabolite profiles were generated using the dataset to clarify the distribution of the identified metabolites between different groups. Figure 2-1 shows that the metabolites

concentrated in the middle of the heatmap tended to be present in high concentrations in hot-natured herbs and in low concentrations in cold-natured herbs. However, few herbs had lower similarities than other herbs, for example Rhizoma zingiberis, Pericarpium zanthoxyli, Rhizoma chuanxiong, and Semen arecae in hot-natured herbs and Radix scutellariae in cold-natured herbs.

Figure 2-2 shows the cluster analysis results of the significant differences in metabolite concentrations between hot/warm- and cold/cool-natured herbs. From the 193 metabolites identified in each herb in Figure 2-1, more than 40 metabolites with significant difference ($p < 0.05$) in concentrations between hot/warm- and cold/cool-natured herbs were selected via cluster analysis. In particular, the concentrations of 2, 5-dihydroxybenzoate, 2-hydroxypentanoate, n-acetylglucosamine, and uracil were significantly higher in hot/warm-natured herbs than in cold-natured herbs ($p < 0.01$). In contrast, glutamine concentration was significantly higher in cold-natured herbs than in hot/warn-natured herbs ($p < 0.01$) (Figure 2-2).

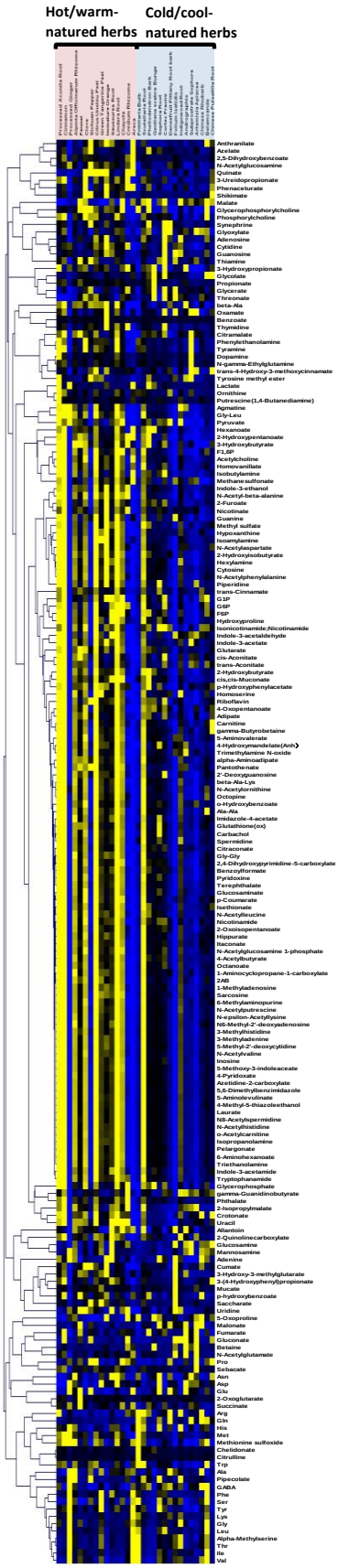

Figure 2-1: Heatmap based on the 193 identified compounds from 30 extracts of Chinese herbs

Rows represent compounds and columns represent the Chinese herb samples. The orange box groups the 15 hot/warm-natured herbs and the blue box groups the 15 cold/cool-natured herbs. Color key indicates the relative concentrations of the identified compounds: yellow indicates higher concentrations, black indicates medium concentrations, and blue indicates lower concentrations. Each herb had three duplicate samples.

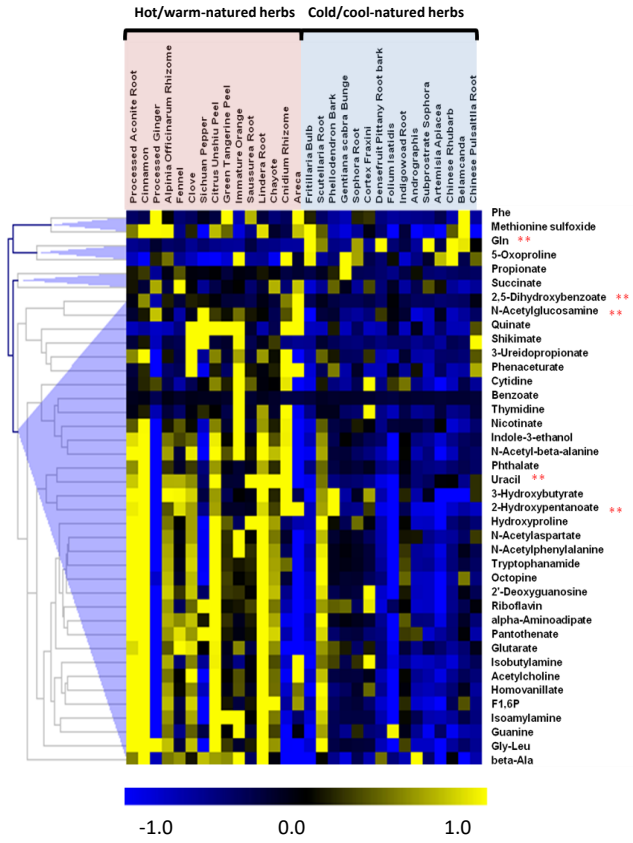

Figure 2-2 Heatmap cluster analysis of the metabolites with significant differences ($p < 0.05$) between the varied groups of hot- and cold-natured herbs

Rows represent metabolites and columns represent herbs. The orange box groups the 15 hot/warm-natured herbs and the blue box groups the 15 cold/cool-natured herbs. Color key indicates the relative concentrations of the identified compounds: yellow indicates higher concentrations, black indicates medium concentrations, and blue indicates lower concentrations. In addition, the p values highlighted with two stars are less than 0.01.

2.3.2 PCA of the charged metabolites in TCMs

As a decomposition approach, PCA allowed the original metabolite data to be reduced to a few principal components of the data to obtain more detailed metabolic variations among the herbs. The PCA score plots (blue for cold/cool-natured herbs and red for hot/warm-natured herbs) and loading plots of the 30 Chinese herbs are presented in Figure 2-3. The first two principal components accounted for 58% of the overall variability. PC1 scores (50.1%) revealed that the spectra of hot/warm-natured and cold/cool-natured herbs were separate, except for that of individual herbs (Rhizoma Zingiberisand Semen Arecae). Overall, except for some deviating data points, the metabolite scores of the hot/warm-natured herbs drifted toward the positive axis, whereas the scores of the cold/cool-natured herbs were focused on the negative axis. Meanwhile, the loading score plots showed that 20 kinds of amino acids contributed to the negative axis, agreeing with the score plots of cold/cool-natured herbs. It seemed that there were respective differences between hot/warm-natured and cold/cool-nature herbs. As indicated by the results, the amino acid concentration was in fact closely related to cold/cool-natured herbs.

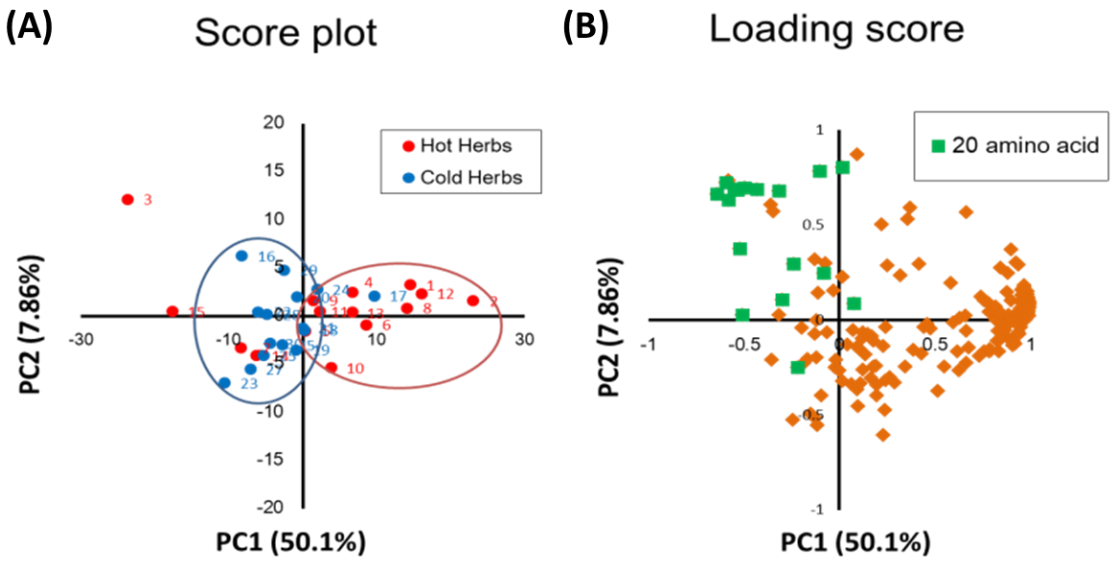

Figure 2-3 Principal component analysis

Score plots (A) and loading scores (B) (PC1 vs. PC2) of the Chinese herbs. The x-axis is principal component 1 (PC1) and the y-axis is principal component 2 (PC2). PC1 and PC2 describe around 50.1% and 7.86% of the total variability, respectively. In the score plot, red represents hot/warm-natured herbs (Hot Herbs) and blue represents cold/cool-natured herbs (Cold Herbs). In addition, the numbers correspond to the names of the herbs in Table 1. In the loading score, the green squares represent the 20 basic amino acids and the orange diamonds represent all other metabolites.

2.3.3 Molecular similarity analysis

Because most of the compounds were derived from a common skeleton building block in the plant metabolic network, the structural similarity of compounds might play an important role in identifying the herb as hot- or cold-natured. Therefore, a hierarchical tree constructed using cluster analysis was investigated to support compound information on relationships with the properties of Chinese herbs. Using the Tanimoto coefficient, the extracted information of the selected 193 metabolites from PubChem Compound was used to calculate the structural similarity between the samples. The samples were arranged into a hierarchy by grouping the common structure of the metabolites (Figure 2-4). In addition, after assigning the major metabolites, the relative concentrations of these metabolites were measured to calculate the mean values of hot- and cold-natured herbs. By comparing with mean values, the relative ratios of cold to hot were calculated to observe the contributions to each group. The results showed that although a non-specific structure was generally observed between cold- and hot-natured herbs, the nucleotides in the red box accounted for a large proportion in most hot-natured herbs.

Next, we visualized the distribution of nucleosides and related concentration of compounds in both hot- and cold-natured herbs using a box plot (Figure 2-5). Thymidine, uridine, cytidine, 1-methyladenosine, N6-methyl-2′-deoxyadenosine, adenosine, guanosine, and uracil were slightly more distributed in hot-natured herbs (pink) than in cold-natured herbs (blue). Soluble nucleotides and analogs are the most important bioactive ingredients in some TCMs[60].

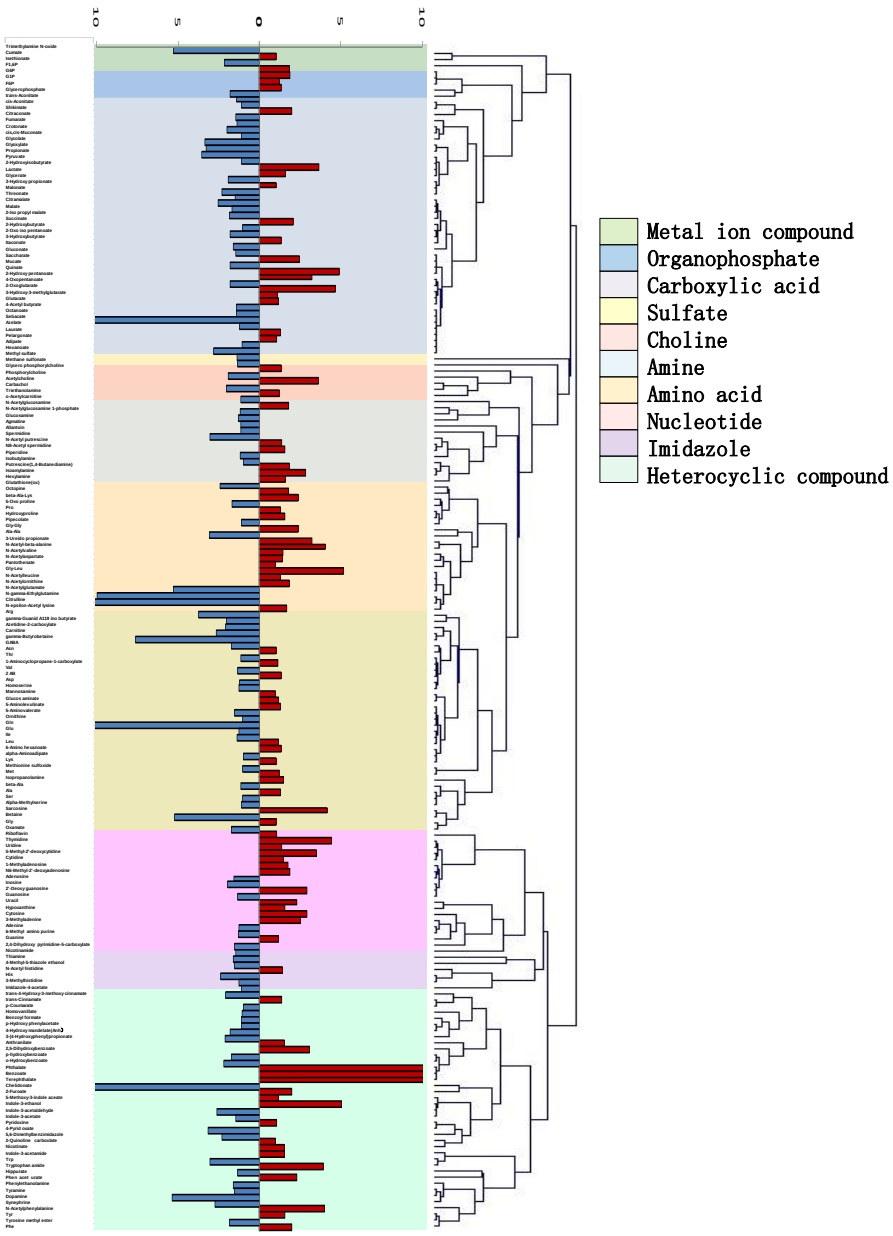

Figure 2-4 Molecular structure similarity of the metabolites and the metabolite content ratio of cold- to hot-natured herbs

The hierarchical tree is constructed using the results of Tanimoto coefficients, and the similarity approach between the molecules of various metabolites is distance-based. The common structure of each classification is represented on the right side of the hierarchical tree. For easy comparison of the ratio of cold- to hot-natured herbs, the left vertical bar chart displays these ratios calculated from the average values of each metabolite. The red colored bars indicate the high metabolite concentration in hot/warm-natured herbs and the blue colored bars indicated the high metabolite concentration in cold-natured herbs.

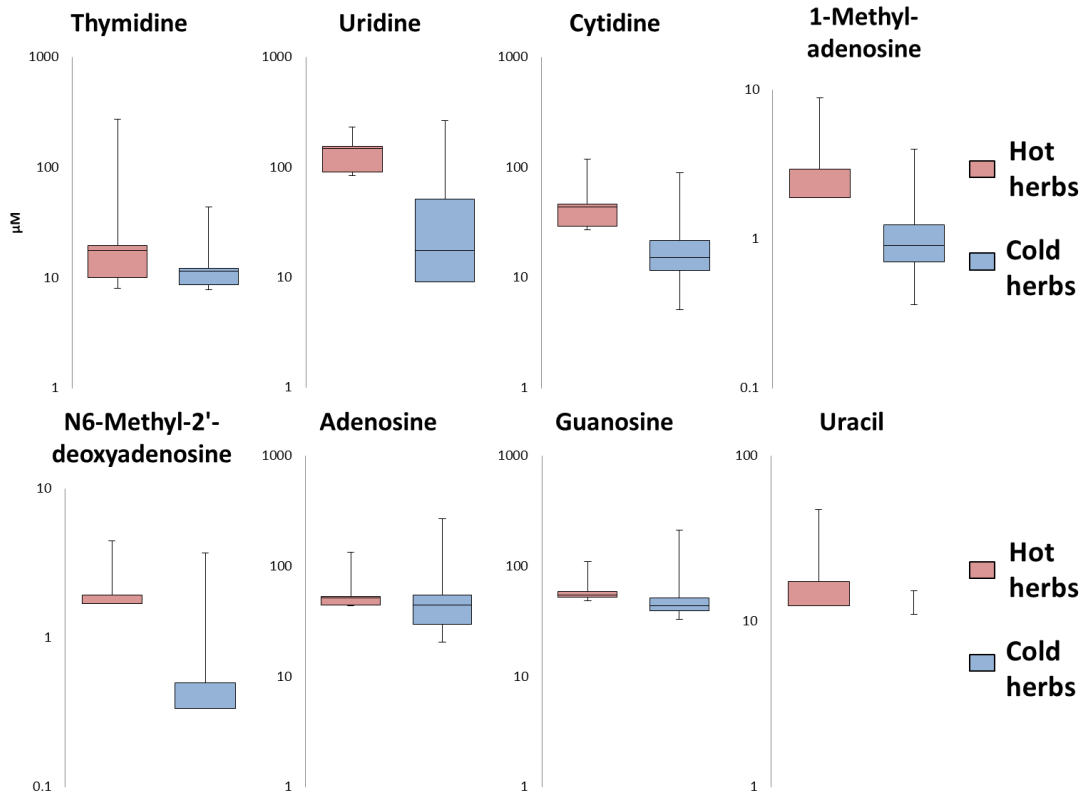

Figure 2-5 Nucleoside metabolites are more widely distributed in hot-natured herbs than in cold-natured herbs

Boxplot shows the concentration of each metabolite in hot- and cold-natured herbs. The pink box expresses the 15 hot-natured herbs (Hot herbs) and the blue box expresses the 15 cold-natured herbs (Cold herbs). Boxplots describe the upper quartile (Q3), median, and the lower quartile (Q1) values. Upper and lower limit whiskers describe maximum and minimum values in the data.

2.4 Discussion

The four-natured principles serve as the reference guide for TCM recipes. However, to date, the underlying mechanism of such different properties on therapeutic effects has not been fully identified at molecular level as a complex research system. This is generally believed to be related to the large number of molecular groups in Chinese herbs. In this study, 15 hot/warm-natured herbs and 15 cold-natured herbs were selected by analyzing their ionic metabolites via CE–TOF/MS detection, followed by multiple statistical analysis approaches to investigate the correlation of properties between each molecular group. The approaches included PCA, discriminant analysis, Tanimoto coefficient analysis, and molecular cluster analysis. In total, 416 metabolites from 30 Chinese herbs were recognized, and it was noted that 193 of the 416 compounds were found in more than 16 herbs. The CE–TOF/MS-based metabolomics with multivariate data analysis enabled the identification of compounds between cold- and hot-natured herbs. Although the levels of compounds, including amino acids, nucleosides, and nucleotides, varied in both cold- and hot-natured herbs due to individual differences, the results via metabolomics PCA, Mann–Whitney U test, and structural similarity analysis still illustrated some regular characteristics among the different groups. Metabolomics analysis of the 193 metabolites indicated significant differences in the contents of the 40 metabolites between hot- and cold-natured herbs (Figure 2-2). In contrast, more amino acid compounds were observed in cold-natured herbs via PCA (Figure 2-3). Comparative analysis of the molecular similarity of the chemical and molecular structures and contents revealed that hot-natured herbs had more number of nucleotides (Figure 2-4).

Many studies have focused on antioxidant activities in cellular or mouse experimental systems[61,62]. However, more quantitative studies of the four natures of Chinese herbs have focused on microelement and chemical compositions[63]. While discussing the effects of chemical compositions on the cold/hot natures of Chinese herbs, the theory of generalized oxidation and reduction was hypothesized to be associated with these kinds of thermal properties[64]. In general, metabolism of the human body can be broadly categorized into catabolism and anabolism[65]. In sharp contrast, cold-natured herbs consist of more amino acid compounds, which are the basic building blocks for

the anabolic processes of cellular growth or function (Figure 2-3). The absorption of amino acids is mainly used for protein synthesis, requiring energy in the form of ATP. Energy consumption leads to a cold effect in nature. Therefore, cold- and hot-natured herbs can be distinguished from the point of view of metabolism. In addition, it has been shown that warm/hot-natured herbs contain more nucleotides and their derivatives (Figure 2-4 and Figure 2-5). Immunity, inflammation, and cancer can all be regulated by extracellular nucleosides[66-68]. Furthermore, based on the functional activities of the metabolites, Liang et al. searched the protein targets of active compounds in the PubChem database and found that immune regulation are more related to hot-natured herbs and that cold-natured herbs possess the tendency to impact cell growth and proliferation[69]. Therefore, the high concentration of nucleosides and analogs in hot-natured herbs may play a role in immune regulation.

Although each herb has different actions and uses, metabolomics analysis indicates that each herb contains the common biologically active ingredients, such as amino acids, organic acids, and nucleoside or nucleotide compounds. Therefore, it should be noted that the different energy natures of hot, warm, cold, and cool are not merely determined by one or a certain class of chemical molecules but by the combined effects of all of ingredients, the so-called molecular groups. Warm/hot-natured herbs are more prevalent in those molecular groups prone to oxidation reactions, such as nucleotides. On the other hand, cold/cool-natured herbs have the predominant components prone to reduction reactions, such as amino acids.

2.5 Conclusions

In this study, to determine the key compounds in Chinese herbs of the four inherent energy properties, CE–TOF/MS-based metabolomics with statistical analysis was performed to measure the metabolites of the 30 selected Chinese herbs. The results show that organic acids and nucleotide compounds are accumulated in the warm/hot-natured herbs, whereas basic amino acids, such as glutamine, and nucleoside compounds are present in higher concentrations in cold-natured herbs. PCA revealed that there are important differences between warm/hot- and cold/cool-natured herbs and that the molecular groups and energy properties of herbs are closely related to each

other. The present results show that our CE–TOF/MS-based metabolomics approach provides a powerful tool to assess the relationship between the molecular mechanisms underlying the four natures of Chinese herbs. This approach will help establish the theoretical basis of TCM or traditional medicine.

Chapter 3 Reprogramming of glutamine metabolism via glutamine synthetase silencing induces cisplatin resistance in A2780 ovarian cancer cells

3.1 Introduction

CDDP, a platinum-based drug, has been a mainstay of treatment in various cancers since it was approved by the U.S. Food and Drug Administration (FDA) in 1978[70-72]. To date, CDDP remains commonly used as a first-line treatment for ovarian cancer in many countries. CDDP binds to nuclear DNA, particularly to the nucleophilic N7 sites of purine bases, with high affinity, thereby activating the DNA damage response[73-75]. However, some cancer cells develop CDDP resistance over time, leading to recurrences in up to 75% of patients with ovarian cancer[76-78]. CDDP-resistant cells often express elevated levels of glutathione (GSH)[79]. Research has shown that the levels of GSH in cancer cells are much higher than those in CDDP-treated cells[80-82]. GSH has high affinity for CDDP and competitively inhibits the binding of CDDP to DNA, causing CDDP resistance[79,83]. Therefore, treatment with a GSH synthesis inhibitor can increase CDDP sensitivity[84].

Alterations in cellular metabolism are a crucial hallmark of cancer[85,86], and cancer cells require both glutamine and glucose for their proliferation[87]. Glutamine contributes to the synthesis of not only nucleotides, amino acids, and proteins, but also of GSH, which is important for antioxidant defense[80]. Glutamine is the most abundant amino acid in serum, but it is often severely depleted in growing tumors due to nutrient-limited environments, and glutamine starvation may lead to rapid cancer cell death[80,82,88]. Extracellular glutamine is transported into cells and converted into glutamate by glutaminase (GLS). Glutamate is in turn used for α-ketoglutarate (α-KG) synthesis by glutamate dehydrogenase (GLUD). Conversely, glutamate is metabolized into glutamine by glutamine synthetase (GS), which is encoded by glutamate ammonia ligase (GLUL). The levels and functions of GS in tumors vary depending on the cellular context[89].

Low-invasive ovarian cancer cells express high levels of GS, whereas highly invasive ovarian cancer cells express low levels of GS[90]. Meanwhile, GS fuels nucleotide biosynthesis and facilitates growth of various cancer cells[83,91-93].

Although recent research has revealed a relationship between CDDP resistance and glutamine metabolism, the exact mechanism is yet to be elucidated[94-98]. A preliminary hypothesis is that CDDP-resistant cells upregulate GSH production from glutamine, thereby attenuating CDDP-induced cytotoxicity. However, key factors that regulate the "resistance system" in cancer cells remain to be identified. Metabolome analysis is one of the powerful approaches to understanding the molecular mechanisms by which cancer cells acquire malignant potential[99].

This study aimed to determine the mechanisms by which ovarian cancer cells acquire CDDP resistance. Towards this goal, we conducted CE-TOF/MS[49,100] to quantify the central carbon metabolites and amino acids in the human ovarian epithelial cancer cell line A2780 and the CDDP-resistant daughter cell line A2780cis and then performed glutamine metabolic flux analysis. Considering the higher levels of glutamine and GSH in CDDP-resistant cells, we hypothesized that reprogramming of glutamine metabolism contributes to CDDP resistance in cancer cells.

3.2 Methods

3.2.1 Materials

Cisplatin (Wako), 3-(4,5-dimethylthiazol-2-yl)-2,5-diphenyltetrazolium bromide (MTT) (Sigma-Aldrich), and Compound 968 (Merck Millipore) were dissolved in phosphate-buffered saline (PBS) and filtered through a 0.22-μm filter. 5-aza-2'-deoxycytidine (5-aza-dC; Tokyo chemical industry) was initially dissolved in dimethyl sulfoxide (DMSO) and further diluted with culture medium.

3.2.2 Cell culture

The human ovarian cancer cell line A2780 (catalog no. 93112519) and the CDDP-resistant cell line A2780cis (catalog no. 93112517) were purchased from

European Collection of Cell Cultures (ECACC) General Cell Collection in 2013. Cell lines were shown to be mycoplasma free using the Mycoalert kit from Lonza. A2780 and A2780cis cells[101,102] were maintained in Roswell Park Memorial Institute (RPMI) 1640 medium (Sigma-Aldrich, Co. R8758) supplemented with 10% heat-inactivated fetal bovine serum (Equitech-bio) and an antibiotic-antimycotic mixed solution (Nacalai Tesque, Inc.). A2780cis cells were maintained in the presence of 1 μM CDDP to maintain CDDP resistance and cultured in the absence of CDDP for 24 h prior to each experiment. For glutamine starvation conditions, RPMI 1640 medium (Sigma-Aldrich, Co. R0883) were used. All cells were grown at 37°C with 5% CO_2.

3.2.3 MTT assay

Cell viability was assessed using the MTT assay as follows. The cells were seeded in 96-well microtiter plates (4×10^3 cells per well) and cultured for 24 h. For exposure to CDDP and compound 968, cells were cultured for an additional 48 h. For cell counting, 20 μL of MTT solution (5 mg/mL) was added to the culture medium, and cells were further cultured for 3 h to generate formazan crystals that were dissolved in 100 μL of DMSO after the culture medium had been removed. Viability was calculated from the absorbance of MTT formazan at 570 nm with a background correction of 690 nm using a TECAN microplate reader with Magellan software (Männedorf). The IC_{50} of CDDP after 48 h was calculated based on the viability curve.

3.2.4 Metabolite extraction and standards

Cells were seeded in 6-well plates (2×10^5 cells in 2 mL of medium) and cultured in regular medium with CDDP or low-glutamine medium for 48 h or the indicated time periods. For flux analysis, 1, 3, 6, and 12 h before sampling, the medium was replaced with medium containing ^{13}C-labeled glutamine.

Sampling was performed by washing the cells twice with 5% mannitol solution, covering with 600 μL of methanol containing 25 μM internal standards (L-methionine sulfone, 2-(N-morpholino)-ethanesulfonic acid, and D-camphor-10-sulfonic acid), and homogenizing for 10 min to inactivate cellular enzymes. The cell-ethanol mixture was collected and mixed with Milli-Q water and chloroform in a 2:1:2 ratio. The resulting

solutions were then centrifuged at 10,000 *g* for 3 min. The aqueous layers were collected for centrifugal filtration though 5-kDa cutoff filters (Merck Millipore) at 9,100 *g* for 3 h. The extracted metabolites were concentrated using a centrifugal concentrator. The concentrated metabolites were dissolved in 25 μL of Milli-Q water containing 200 μM of the reference compounds (3-aminopyrrolidine and trimesate).

All metabolite standards were dissolved in Milli-Q water to obtain 10 mM or 100 mM stock solutions. Working standard mixtures were prepared by diluting stock solutions with Milli-Q water prior to injection into the CE-TOF/MS. All chemicals used were of analytical or reagent grade.

3.2.5 CE-TOF/MS conditions for cationic and anionic metabolite analyses

The following instrumentation and measurement conditions were used for CE-TOF/MS (Agilent Technologies, Santa Clara, CA, USA) as previously reported[49,99,100]. Briefly, for analyzing cations, a fused silica capillary (50 μm i.d. × 100 cm total length) was used with 1 M formic acid as the electrolyte[49]. Each sample was injected by applying a pressure of 50 mbar for 3 s and a continuous voltage of +30 kV. A solution of 5 mM ammonium acetate and 0.5 μM reserpine in 50% (v/v) methanol in water was used as the sheath liquid at a flow rate of 10 μL/min. ESI-TOFMS was performed in the positive ion mode, and the capillary voltage was set to 4 kV. Automatic recalibration of each acquired spectrum was achieved using the masses of the reference standards ([^{13}C isotopic ion of a protonated methanol dimer (2 MeOH+H)]+, m/z 66.0631) and ([hexakis(2,2-difluoroethoxy)phosphazene +H]+, m/z 622.0290). For analyzing anions, a commercially available COSMO (+) (chemically coated with cationic polymer) capillary (50 μm i.d., 5 cm total length) (Nacalai Tesque, Kyoto, Japan) was used with a 50 mM ammonium acetate solution (pH 8.5) as the electrolyte [100]. Each sample was injected by applying a pressure of 50 mbar for 30 s and a continuous voltage of -30 kV. Methanol/5 mM ammonium acetate (50% v/v) containing 0.1 μM hexakis(2,2-difluoroethoxy)phosphazene was delivered as the sheath liquid at 10 μL/min. ESI-TOFMS was performed in the negative ion mode, and the capillary voltage was set to 3.5 kV. Automatic recalibration of each acquired spectrum was achieved using the masses of the reference standards (^{13}C isotopic ion of deprotonated

deuterated acetic acid dimer (2CD3COOH-H)- m/z 126.076001, Hexakis(2,2-difluoroethoxy)phosphazene +deprotonated deuterated acetic acid (M+CD3COOH-H)- m/z 683.054372). The other conditions were identical to those described previously.

3.2.6 Metabolome data processing

Metabolome data were preprocessed with MasterHands ver.2[53]. The peaks were identified by matching the m/z values and normalized migration times of corresponding external stand compounds. All of the identified peaks were changed manually, and noise-derived peaks were removed based on S/N values. All peak areas were normalized using internal standards, and the concentrations of each compound were calculated according to the relative area of the external standard compound. The average amount of each metabolite per cell was evaluated based on the number of viable cells in each cell line. The number of cells was determined using a hemocytometer.

Hierarchical clustering of metabolite levels for heatmap visualization was performed in MultiExperiment Viewer (MeV)[55].

3.2.7 Western blot analysis

The protein levels of glutamine-related enzymes were determined via Western blot analysis. Briefly, cells were collected using cell scraper, washed once with PBS, and centrifuged at 5,000 rpm for 1 min. Protein extracts were prepared by lysing cells in RIPA Buffer (Nacalai tesque) on ice for 10 min. Protein quantification was performed using a Broadford protein assay kit (BIO-RAD). After determining the protein concentration, protein samples were mixed with 5× loading buffer then boiled for 10 min at 96°C. Samples (20 μg of protein) were separated using SDS-PAGE (7.5% gel) and then transferred to a polyvinylidene difluoride (PVDF) membrane with a Trans-Blot Turbo Transfer System (BIO-RAD).

The membrane was first blocked with PBST containing 4% BSA for 10 min at room temperature. Next, they were incubated with primary antibodies at 4°C overnight and then incubated with secondary antibodies at room temperature for 2 h. The immunoreactive proteins on the membrane were analyzed using ECL detection reagents

and Image Quant LAS 4000 (GE Healthcare). The antibodies used were as follows: anti-GLUL, 1:1,000 (HPA007316, Atlas Antibodies); anti-GLS, 1:2,000 (ab156876, Abcam); anti-β-actin, 1:10,000 (ab8226, Abcam); anti-rabbit IgG HRP-linked antibody, 1:10,000 (Cell Signaling); anti-mouse IgG HRP-linked antibody, 1:10,000 (Cell Signaling).

3.2.8 Knockdown of GS expression

siRNA targeting human GS and negative control siRNA were purchased from Sigma-Aldrich. A2780 cells were separately seeded in 6-well culture plates at a density of 4×10^3 cells/well and cultured for 24 h. For siRNA transfection, complexes of siRNA duplex and Lipofectamine RNAiMAX (Invitrogen) were formed in serum-free medium and added to the culture medium at a final concentration of 25 nM siRNA. For RNA extraction, transfected cells were harvested 48 h after transfection. The siRNA sequences for GS were as follows: 5'-GAUUGGACCUUGUGAAGGAdTdT-3'; 5'-UCCUUCACAAGGUCCAAUCdTdT-3'.

3.2.9 Quantitative real-time polymerase chain reaction (qRT-PCR)

RNA was isolated from cells using RNeasy Mini kit (Qiagen) following the manufacturer's instructions. RNA concentration was qualitatively assessed and quantified using NanoDrop 2000 (Thermo scientific). Total RNA (2 μg) was reverse transcribed to cDNA with a ReverTra Ace qPCR RT Master Mix (TOYOBO). RT-PCR was performed with SYBR Green RT-PCR Master Mix (TaKaRa) on a StepOnePlus Real-Time PCR System (Thermo Scientific). PCR cycles consisted of initial denaturation at 95°C for 30 sec, followed by 40 cycles of 95°C for 30 sec, 95°C for 5 sec, and 60°C for 30 sec. The relative expression of mRNA was calculated using the $2^{-\Delta\Delta Ct}$ method. Data were normalized to the expression of β-actin or RPL27. The sequences of primers used are listed inTable S1Table S1.

3.2.10 DNA demethylation

For DNA demethylation, cells were seeded in 6-well plates at a density of 2×10^5 cells per well). After overnight culture, 2 μM 5-aza-2'-deoxycytidine (5-aza-dC), a DNA methyltransferase inhibitor, was added to the culture medium, and cells were incubated for an additional 72 h. GS expression was determined using RT-PCR.

3.3 Results

3.3.1 Components of glutamine metabolism is increased in CDDP-resistant cells

Drug resistance is one of the most crucial challenges in cancer treatment. We used the CDDP-sensitive human ovarian cancer cell line A2780 and the CDDP-resistant cell line A2780cis, which was obtained by long-term exposure of A2780 cells to increasing concentrations of CDDP[101]. The MTT assay showed that the half-maximal inhibitory concentrations (IC_{50}) for CDDP in A2780cis cells were approximately 20 times greater than those in A2780 cells (Figure 3-1A). The colony formation capability of A2780cis cells was also greater than those of A2780 cells (Figure 3-1B).

These cell lines were also evaluated using CE-TOF/MS to determine the metabolic pathways responsible for CDDP resistance. The 189 metabolites in the major energy metabolism pathway were identified in extracts of A2780 and A2780cis cells using authentic standards. Principal component analysis (PCA) of metabolites revealed global metabolic changes between A2780 and A2780cis cells (Figure 3-1C). The score plots along with the first principal component axis (PC1) showed marked differences between these cell lines. As shown by the volcano plots, the levels of 50 metabolites were increased to 2-fold or more, whereas those of 8 metabolites were decreased to 0.5-fold or less in A2780cis cells compared with those in A2780 cells (Figure 3-1D and Table S2). The most remarkably increased metabolite in A2780cis cells was glutamine, the levels of which were 88-fold higher than those in A2780 cells (Figure 3-1E). In addition, the levels of glutamate and GSH, which are synthesized from glutamine, were also significantly increased in A2780cis cells (Figure 3-1E). This shows that in A2780cis

cells, CDDP resistance was elevated with metabolic changes, including increases in the components of glutamine metabolism.

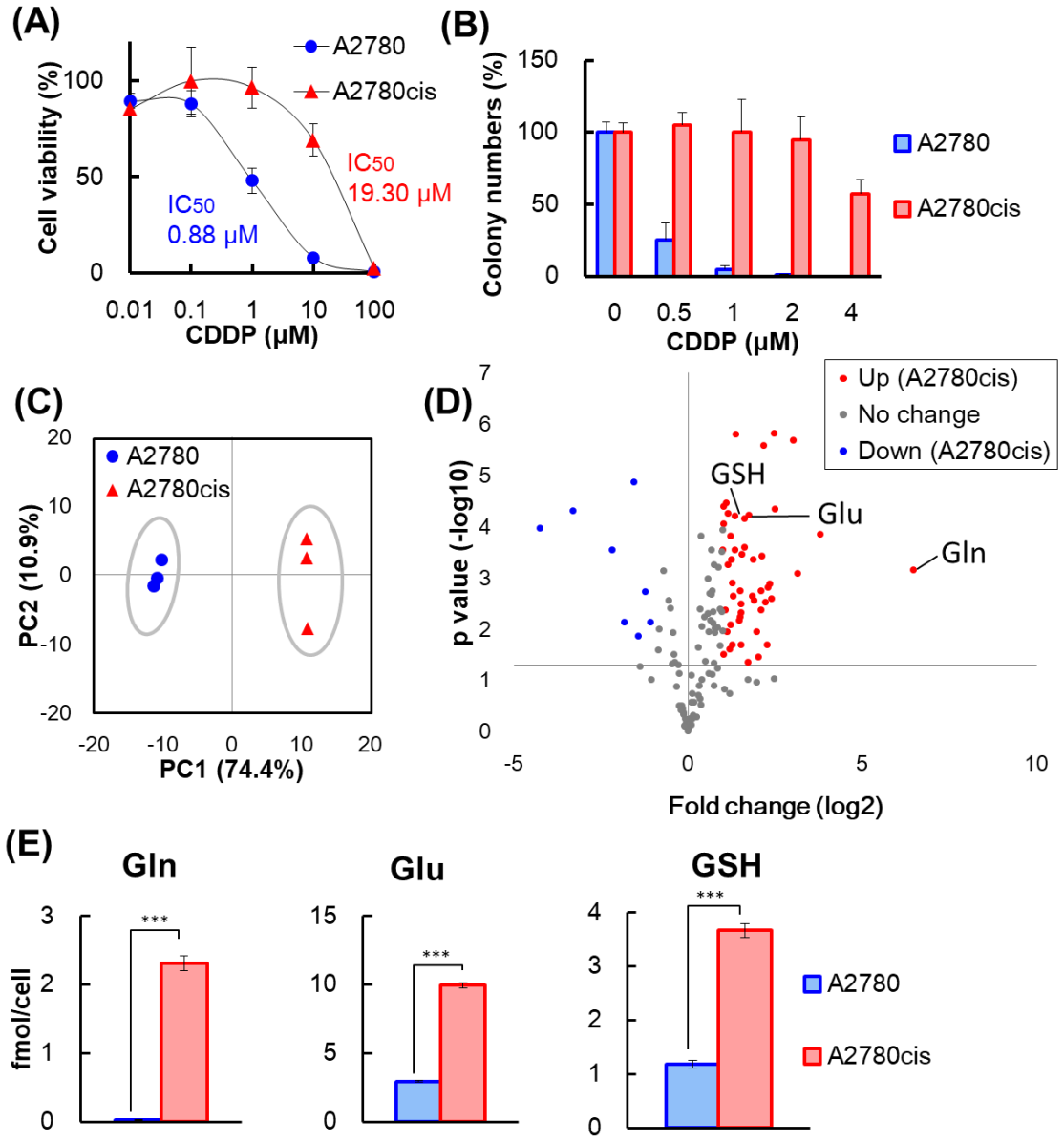

Figure 3-1 Increase in CDDP resistance and global metabolic changes in A2780cis cells

(A) Effects of CDDP treatment on the viability of A2780 and A2780cis cells. Cell viability was measured at 48h after treatment using the MTT assay. (B) For colony formation assays, A2780 and A2780cis cells were cultured in the presence of CDDP (concentrations as indicated). Colonies were counted 9 days after plating. (C) Score plots of principal component analysis (PCA) of 189 intracellular metabolite levels in A2780 and A2780cis cells measured using CE-TOF/MS. The contribution rate of PC1 and PC2 were 74.4% and 10.9%, respectively. (D) Volcano plots with the fold change of each metabolite and p values calculated using the Student's t-test ($p<0.05$). The horizontal axis indicates a p-value (-log10) of 0.05. The averages metabolite levels in

A2780cis cells were compared with those in A2780 cells (n=3). Red dots depict significantly increased metabolites in A2780cis cells. Blue dots depict significantly decreased metabolites in A2780cis cells. Gray dots depict metabolites without significant differences. See also Table S2. (E) Levels of glutamine (Gln), glutamate (Glu), and GSH in A2780 and A2780cis cells. Data are shown as the mean ± SD of the three independent experiments. Statistical significance was determined using the Student's t-test (**$p<0.01$, ***$p<0.001$).

3.3.2 Reprogramming of glutamine metabolism enhances CDDP resistance in ovarian cancer cells

Glutamine as one of the main energy sources is involved in cancer cell proliferation, inhibition of apoptosis, and cell signaling[88,103,104]. Glutamine is converted to glutamate, which is a metabolic intermediate channeled into the tricarboxylic acid (TCA) cycle and GSH synthesis[105]. Taken together with our observations that levels of glutamine and GSH are higher in CDDP-resistant cells, we hypothesized that reprogramming of glutamine metabolism contributes to CDDP resistance in cancer cells. To test our hypothesis, we conducted three experiments.

First, to examine the difference in glutamine metabolism between A2780 and A2780cis cells via metabolic flux analysis using glutamine isotopically labeled at all five carbon atoms ($^{13}C_5$-glutamine). For this analysis, we cultured these cell lines in medium containing labeled glutamine and determined the levels of metabolites produced from labeled glutamine using CE-TOF/MS. As expected, the levels of $^{13}C_5$-labeled glutamine were similar in both cell lines, suggesting that glutamine incorporation was not changed in A2780 and A2780cis cells (Figure 3-2A, orange). Meanwhile, the levels of labeled TCA cycle metabolites ($^{13}C_1$–$^{13}C_5$), including α-KG, were lower in A2780cis cells than in A2780 cells. (Figure 3-2B, and Figure S1). In contrast, labeled GSH was actively produced from labeled glutamine in A2780cis cells (Figure 3-2C). These results suggest that glutamine is preferentially involved in GSH production in CDDP-resistant cells.

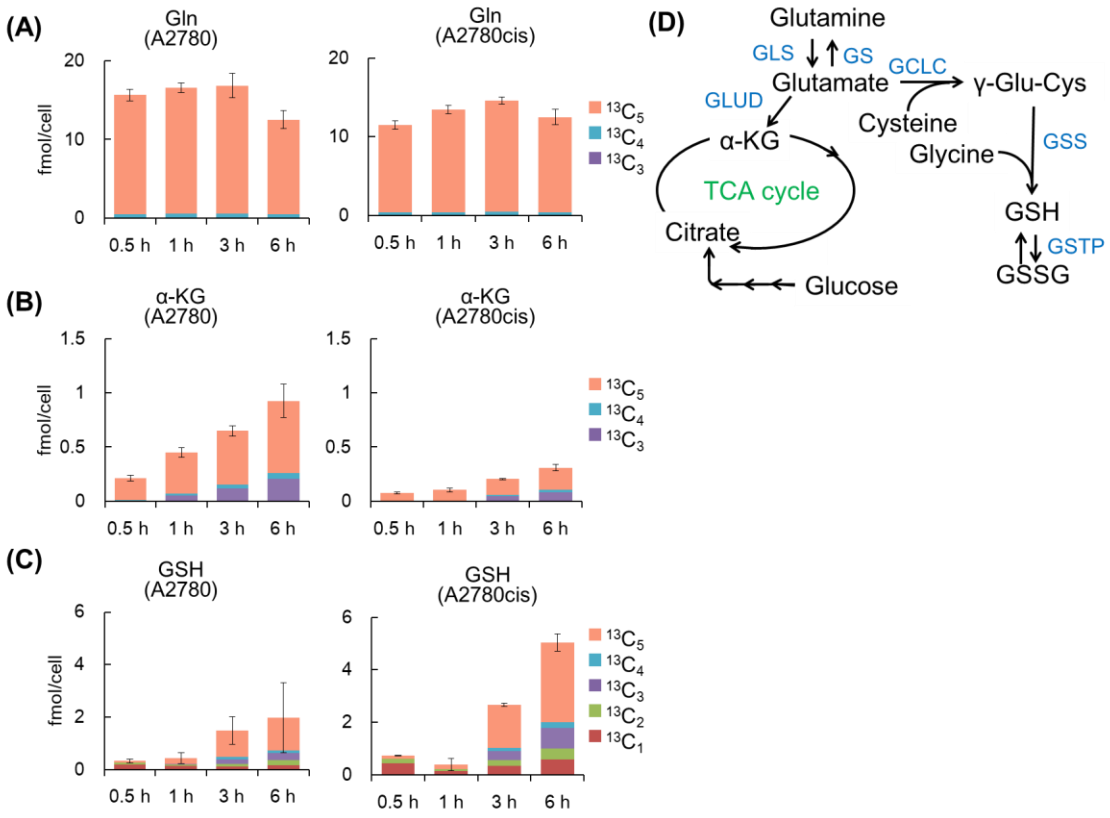

Figure 3-2 Metabolic flux analysis using isotopically labelled glutamine in A2780 and A2780cis cells

(A, B, and C) Isotopologue distribution of metabolites in A2780 and A2780cis cells. Cells were incubated with medium containing glutamine isotopically labeled at all five carbon atoms ($^{13}C_5$-glutamine) for the indicated time periods. Carbon fluxes from glutamine to Glu, GSH, and α-ketoglutarate (α-KG) were determined using CE-TOF/MS. Each bar color corresponds to the number of ^{13}C replaced with 12C in the metabolites. Data are shown as the mean ± SD of three independent experiments. (D) A pathway map of glutamine metabolism. Metabolites and catalytic enzymes are shown in black and blue, respectively. The colored dots show the ^{13}C isotopically labeled metabolites, and the color corresponds to the icons in Figure 3-2A–C on the left.

Second, we used CE-TOF/MS to analyze the metabolic profiles of A2780 and A2780cis cells cultured under glutamine starvation conditions. In agreement with the results of the first experiment, the levels of glutamate and GSH in A2780cis cells were significantly decreased under glutamine starvation conditions, while those in A2780 cells were not affected by glutamine starvation (Figure 3-3A). We also found that levels of various metabolites were changed by glutamine starvation in both cell lines (Table S3-6). These results indicate that glutamine starvation causes metabolic reprogramming.

Third, we assessed CDDP resistance of A2780 and A2780cis cells in the presence or absence of glutamine. The viability of A2780 cells was decreased not only by CDDP treatment alone, but also by glutamine starvation alone, suggesting that A2780 cells depend on glutamine to sustain their proliferation (Figure 3-3B left). In contrast, the viability of A2780cis cells was neither drastically affected by CDDP treatment alone nor glutamine starvation alone (Figure 3-3B right). Importantly, however, glutamine starvation reduced the viability of A2780cis cells in the presence of CDDP. The effect of glutamine starvation on the viability of A2780cis cells was also greater than those of A2780 cells in the presence of CDDP. These results indicate that A2780cis cells depend on glutamine to induce CDDP resistance.

The results of these three experiments collectively support the hypothesis that glutamine is utilized preferentially for GSH production rather than for TCA cycle metabolite production in A2780cis cells. This reprogramming of glutamine metabolism enhances CDDP resistance.

The result that glutamine metabolism plays an important role in CDDP resistance prompted us to examine the effect of treatment with a glutamine metabolism inhibitor on CDDP resistance. Accordingly, we treated cells with a constant concentration of CDDP (10 μM) and various concentrations of compound 968, a GLS inhibitor, and analyzed cell viability. Consistent with the results presented in Figure 3-3B, the viability of A2780cis cells in the presence of CDDP was decreased by compound 968 treatment in a concentration-dependent manner (Figure 3-3C). These results show that treatment with a GLS inhibitor enhances the cytotoxic effects of CDDP on CDDP-resistant cells.

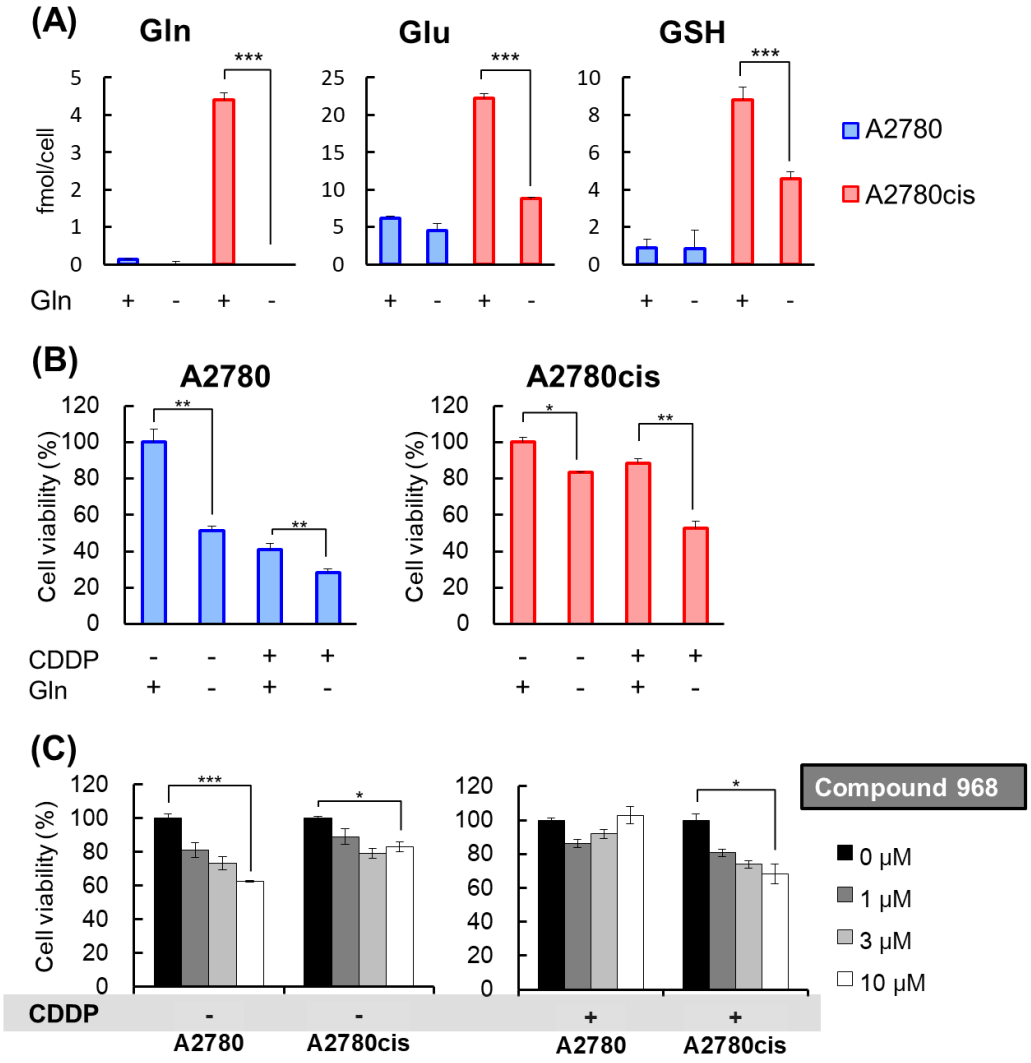

Figure 3-3 Glutamine starvation reduces the GSH level and CDDP resistance in A2780cis cells

(A) Levels of Gln, Glu, and GSH in A2780 and A2780cis cells cultured in the presence (+) or absence (-) of glutamine. (B) Effects of glutamine starvation on CDDP resistance. A2780 and A2780cis cells were treated with 3 μM CDDP in the presence (+) or absence (-) of glutamine for 48 h. (C) A2780 and A2780cis cells were cultured for 48h in medium containing CDDP (0 or 10 μM) and the GLS inhibitor compound 968 (0, 1, 3, or 10 μM). Cell viability was measured using the MTT assay. Data are shown as the mean ± SD of the three independent experiments. The differences were analyzed by using the Student's t-test (*p<0.05, **p<0.01, ***p<0.001).

3.3.3 CDDP resistance in A2780cis cells is caused by DNA methylation-mediated silencing of GS expression

As shown in Figure 3-3B and Figure 3-3C, CDDP-induced cytotoxicity against A2780cis cells was enhanced by glutamine starvation or GLS inhibitor treatment. Therefore, we next examined the expression of glutamine metabolism enzymes. Unexpectedly, real-time polymerase chain reaction (RT-PCR) and Western blot analyses showed that there were no significant differences in the levels of GLS between A2780 cells and A2780cis cells (Figure 3-4A). Meanwhile, GLS expression was induced in the presence of glutamine, a substrate for GLS, in both cell lines (Figure 3-4B). In addition, both cell lines expressed similar levels of GLUD1, GCLC, GSS, and GSTP1, a major drug-metabolizing enzyme [106,107] (Figure 3-4A). We also performed western blotting to examine the expression level of GS in medium with normal glutamine concentration and medium without glutamine.

Interestingly, we found that GS expression was almost completely suppressed in A2780cis cells (Figure 3-4A), whereas A2780 cells expressed a detectable level of GS in the presence of glutamine and a higher level of GS in the absence of glutamine (Figure 3-4B). Thus, it is believed that the absence of glutamine causes cells to express a higher level of GS, which supplements glutamine level in the cells. However, GS expression did not increase in A2780cis cells even in the absence of glutamine. Bott et al. recently reported that the GS promoter is methylated in human mammary epithelial cells and that GS expression is induced by Myc-mediated promoter demethylation [92]. Therefore, to determine whether suppression of GS expression in A2780cis cells is due to DNA methylation, we treated A2780cis cells with 5-aza-2'-deoxycytidine (5-Aza-dC), an inhibitor of DNA methyltransferases, and analyzed GS expression using RT-PCR. As expected, GS expression was markedly increased by 5-Aza-dC treatment, indicating that GS expression is suppressed by DNA methylation (Figure 3-4C). We further investigated whether 5-Aza-dC treatment attenuates CDDP resistance in A2780cis cells. We treated A2780cis cells with a constant concentration of CDDP (10 μM) and various concentrations of 5-Aza-dC and found promising findings. The viability of A2780cis cells in the presence of CDDP was decreased by 5-Aza-dC treatment in a

concentration-dependent manner (Figure 3-4D). This result demonstrates that CDDP resistance in A2780cis cells is diminished by 5-Aza-dC treatment.

Finally, to clarify the role of GS in CDDP resistance, we knocked down GS expression in parental A2780 cells, which express GS and are CDDP sensitive, and evaluated cell viability in the presence of various concentrations of CDDP (Figure 3-4E). Consistent with the results that CDDP-resistant A2780cis cells scarcely expressed GS, GS knockdown in A2780 cells caused an approximately two-fold increase in the IC_{50} value for CDDP (Figure 3-4F). Collectively, these results indicate that CDDP resistance in A2780cis cells is induced, at least in part, by DNA methylation-mediated silencing of GS expression.

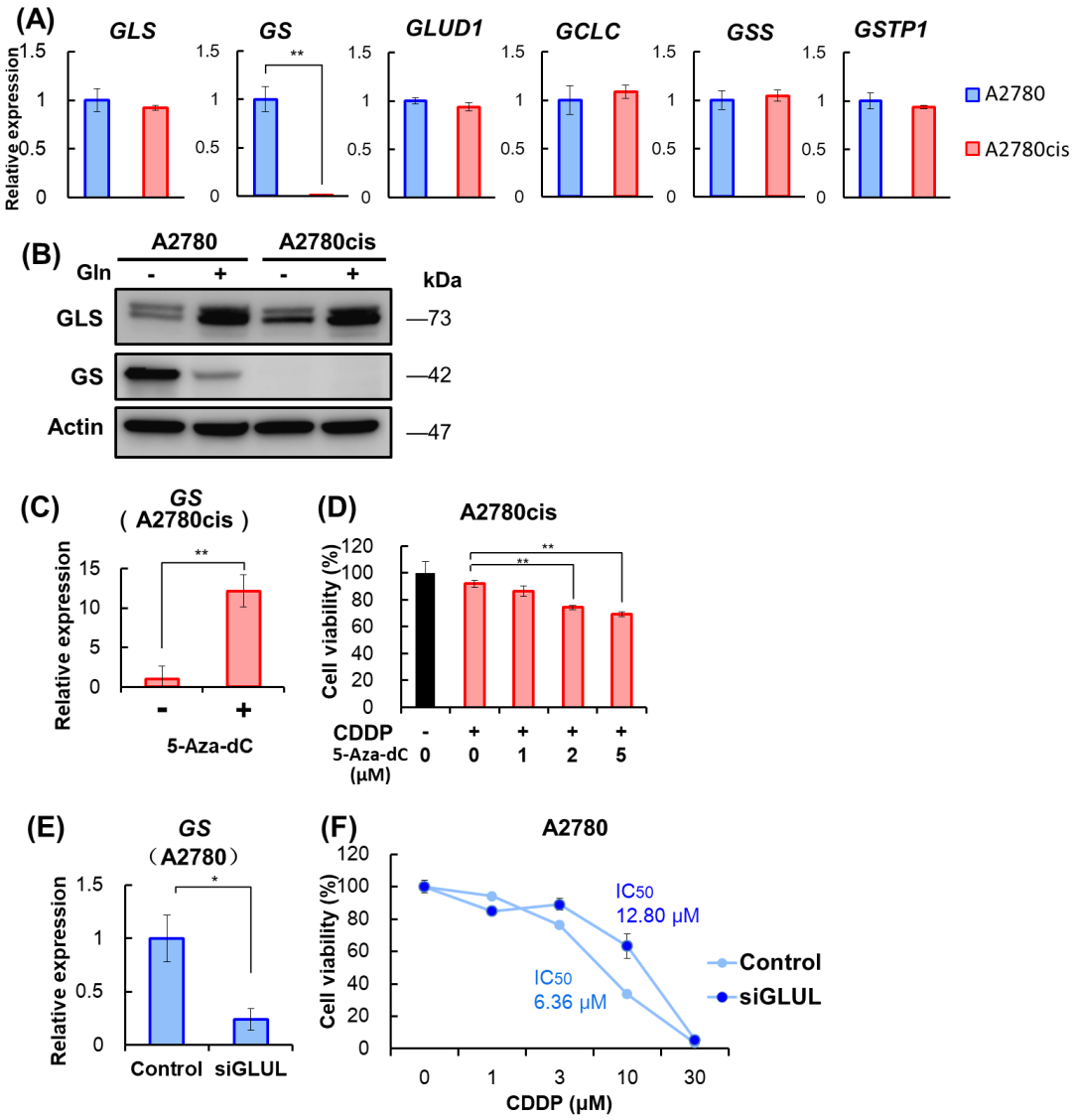

Figure 3-4 CDDP resistance in A2780cis cells is caused by DNA methylation-medicated silencing of GS expression

(A) RT-PCR analysis of glutamine metabolism enzymes. (B) Western blotting of glutamine metabolism enzymes. "+"indicates culture medium with normal glutamine concentration, and "–" indicates culture medium without glutamine. Cells were cultured in the absence or presence of glutamine for 48 h. (C) RT-PCR analysis of GS expression in A2780cis cells. Cells were cultured for 72 h in the absence or presence of 5-Aza-dC (2 μM). (D) Effects of 5-Aza-dC on CDDP-induced cytotoxicity. A2780cis cells were cultured for 72 h in medium containing CDDP (0 or 10 μM) and 5-Aza-dC (0, 1, 2, or 5 μM). Cell viability was measured using the MTT assay. (E) Confirmation of GS knockdown in A2780 cells using RT-PCR analysis. (F) Effects of CDDP knockdown on CDDP-induced cytotoxicity. A2780 cells transfected with control siRNA or GS siRNA were cultured for 72 h in the presence of CDDP (concentrations as indicated). Cell viability was measured using the MTT assay. Data are shown as the mean ± SD of the

three independent experiments. The differences were analyzed using the Student's t-test or one-way ANOVA with Dunnett's multiple comparison (*$p<0.05$, **$p<0.01$).

3.4 Discussion

Through catalyzing the formation of glutamine from glutamate and ammonia, GS functions in various processes in cancer cells, including nucleotide biosynthesis, cell proliferation[83,91,93], and cell invasion[108]. However, the roles of GS in CDDP resistance in cancer cells have not been elucidated. In this study, we found global metabolic changes in CDDP-resistant ovarian cancer cells. First, levels of glutamine, glutamate, and GSH, which is associated with drug resistance, were higher in A2780cis cells than those in A2780 cells (Figure 3-1E). Second, levels of TCA cycle metabolites synthesized from glutamine were lower in A2780cis cells than those in A2780 cells (Figure 3-2B; Figure S1). To our best knowledge, this is the first study to report the importance of glutamine metabolic reprogramming in CDDP resistance.

In addition, we found that glutamine starvation reduced the levels of glutamine, glutamate, and GSH and, accordingly, CDDP resistance in A2780cis cells (Figure 3-3A; Figure 3-3B). Treatment of A2780cis cells with compound 968, a GLS inhibitor, also diminished CDDP resistance (Figure 3-3C). Furthermore, treatment of A2780cis cells with 5-Aza-dC restored the expression of GS and reduced CDDP resistance (Figure 3-4C and Figure 3-4D). In summary, glutamine starvation, GLS inhibition, and 5-Aza-dC treatment reduced CDDP resistance in A2780cis cells. These results indicate that GSH production from glutamine plays a crucial role in the development of CDDP resistance. Consistent with these observations, GS knockdown in CDDP-sensitive A2780 cells induced CDDP resistance (Figure 3-4F).

Based on our results, we proposed a hypothesis for the development of CDDP resistance in ovarian cancer cells (Figure 3-5). In CDDP-sensitive cells, both GLS and GS are expressed, and low levels of GSH are produced from glutamate. In contrast, in CDDP-resistant cells, GS expression is suppressed by DNA methylation, while GLS expression is maintained. Thus, high levels of GSH are produced, and levels of TCA cycle metabolites synthesized from glutamine are decreased. This reprogramming of glutamine metabolism causes CDDP resistance. The mechanisms and functional roles of decreases in levels of glutamine-derived TCA cycle metabolites remain to be elucidated in CDDP-resistant cells. However, we speculate that in addition to GS, other genes may also be silenced by DNA methylation. These alterations in gene expression may

contribute to a metabolic shift from TCA cycle metabolite synthesis to GSH synthesis. This reduction of TCA cycle activity might cause cell growth suppression, a decrease in CDDP-induced DNA damage, and CDDP resistance.

Our present study shows that GS expression is almost completely suppressed via DNA methylation in CDDP-resistant A2780cis cells (Figure 3-4A, B, C). GS knockdown in CDDP-sensitive A2780 cells induced CDDP resistance (Figure 3-4F). Interestingly, Yang et al reported that low-invasive ovarian cancer cells express high levels of GS, whereas highly invasive ovarian cancer cells express low levels of GS[108]. Other studies reported that daunorubicin-resistant acute lymphoblastic leukemia cells lack GS expression[109]. In addition, GS knockdown in non-small cell lung cancer and hepatocellular carcinoma cells enhances resistance to gefitinib and sorafenib, respectively[110,111]. GS knockout in non-small-cell lung carcinoma cells also increases resistance to pazopanib and docetaxel[112]. Thus, we infer that GS inactivation is a crucial step in acquiring malignant potential, including drug resistance, in various cancers.

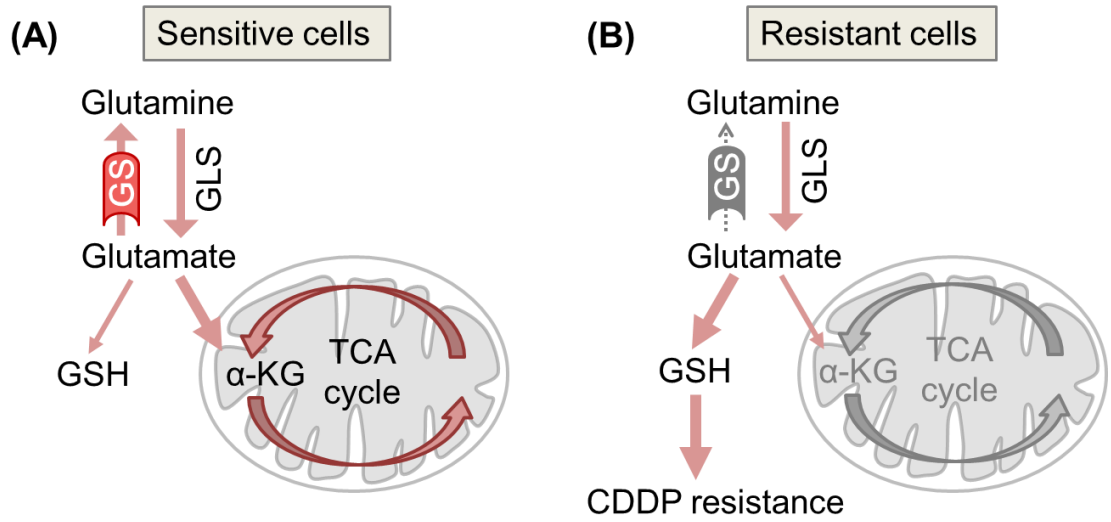

Figure 3-5 A model for CDDP resistance development via reprogramming of glutamine metabolism in ovarian cancer cells

(A) In CDDP-sensitive cancer cells, both GLS and GS are expressed, and low levels of GSH are produced from glutamate. (B) In contrast, in CDDP-resistant cells, GS expression is suppressed by DNA methylation, whereas GLS expression is maintained, and thereby high levels of GSH are produced. This reprogramming of glutamine metabolism causes CDDP resistance.

3.5 Conclusions

Our results highlight the importance of glutamine metabolism in CDDP resistance in ovarian cancer cells. We found that levels of glutamine, glutamate, and GSH in A2780cis cells were significantly higher than those in A2780 cells. GS expression was almost completely suppressed in A2780cis cells. In addition, treatment of A2780cis cells with 5-aza-dC restored GS expression and reduced CDDP resistance. Thus, targeting glutamine metabolism, particularly with DNA methyltransferase inhibitors, could be a promising strategy to overcome chemotherapy resistance in various cancers.

Chapter 4 Metabolic flow analysis coupled with proteomic analysis revealed the effect of glutamine synthetase in cancer cells

4.1 Introduction

Glutamine is a pleiotropic molecule in cancer cell metabolism, and it is known that several cancer cells use glutamine excessively. Glutamine is used to promote cell proliferation and maintain survival, particularly in malnutrition and poor angiogenesis[113]. Glutamine provides carbon and nitrogen to various cell biosynthesis, amino acids, lipids, nucleotides, etc. In addition, it supplements the tricarboxylic acid (TCA) cycle in the mitochondria and produces NADPH and ATP. Moreover, it provides the substrate of GSH synthesis and is used to reduce intracellular reactive oxygen species (ROS)[114,115]. GS is the only enzyme involved in the *de novo* synthesis of glutamine, and when the intracellular glutamine concentration is low, GS is upregulated to maintain glutamine concentration[83]. Cancer cells use excessive glutamine; however, their glutamine is converted into glutamate, which is catalyzed by glutaminase (GLS) to support cell proliferation-related biosynthesis[116]. This metabolic trend is known as glutaminolysis. Cancer cells that overexpress GLS depend on glutamine, making them less likely to survive in the absence of glutamine. GLS treatment strategies have been proposed. Inhibitors such as BPTES, CB-839, and 968, for example, have been developed, and CB-839 is currently in clinical trials[117]. Some cancer species, however, are resistant to GLS inhibitors, and it is known that most of them are highly expressed in GS (encoded by *GLUL*; *glutamate-ammonia ligase*)[118]. Furthermore, it has been demonstrated that GS knockdown can suppress GLS expression, whereas GLS does not affect GS levels[119]. Cancer cells with high GS are self-sufficient in glutamine and can survive in the absence of glutamine. In addition, existing studies on GS expression and functions are different for each cancer type. Overall, the lack of GS is considered to be associated

with high GLS activity, high dependence on glutamine, cancer infiltration, and drug resistance[82].

In our previous study comparing sensitive cell lines of ovarian cancer cell lines and resistant cell lines to CDDP, the resistant strain A2780cis had a very low GS expression compared with sensitive cell lines. In A2780 cells, the parent cell line, reduced levels of glutamine in the media clearly increased GS expression; however, this trend was not observed in the resistant cells. Furthermore, the knockdown of GS by siRNA shows an increase in CDDP resistance. We found that after the glutamine entered the cell membrane, the CDDP-resistant A2780 cell line produced more GSH and that GSH had a stronger antioxidant effect, resulting in resistance. On the other hand, we suggest that CDDP-sensitive cell lines send more glutamine into mitochondria and have a favorable metabolic environment for unrestricted cell proliferation. In other words, GS is thought to be like a switch of the metabolism upstream[120]. To better understand the possible functionality of GS in cancer cells, we knocked down GS in more cancer cell lines with varying levels of GS expression and examined their drug resistance, proteomics changes, and metabolomics changes in the following study.

4.2 Materials and Methods

4.2.1 Cell culture

Human ovarian cancer cell line A2780 and human lung cancer cell lines A549 and MOR were purchased from the European Collection of Authenticated Cell Cultures (ECACC). A2780 and MOR cells were maintained in Roswell Park Memorial Institute 1640 (RPMI 1640) (Sigma-Aldrich, Co. R8758) medium supplemented with 10% heat-inactivated fetal bovine serum (FBS) (Equitech-bio). The A549 cells were maintained in Dulbecco's Modified Eagle Medium (DMEM) (Nacalai, Co. 09891–25) supplemented with 10% FBS. The cell lines were incubated in a humidified atmosphere of 5% CO_2 at 37 °C.

4.2.2 MTT assay

Cell viability was evaluated using the MTT assay as follows. The cells were seeded in 96-well microtiter plates (4×10^3 cells per well) and cultured for 24 h. For exposure to CDDP and carboplatin (CBDCA), cells were cultured for an additional 48 h or 72 h. For cell counting, 20 μL of MTT solution (5 mg/mL) was added to the culture medium, and cells were further cultured for 3 h to generate formazan crystals which were dissolved in 100 μL of dimethyl sulfoxide (DMSO) after the culture medium had been removed. Viability was determined from the absorbance of MTT formazan at 570 nm with a background correction at 690 nm using a TECAN microplate reader with Magellan software (Männedorf).

4.2.3 Real-time quantitative PCR

Total RNA was extracted from cells using an RNeasy Mini kit (Qiagen) according to the manufacturer's instructions. Subsequently, 2 μg of extracted RNA was reverse transcribed to cDNA with ReverTra Ace qPCR RT Master Mix (TOYOBO). Target mRNA was quantified using SYBR Green RT-PCR Master Mix (TaKaRa) with StepOnePlus Real-Time PCR System (Thermo Scientific). PCR cycles included initial at 95 °C for 30 sec, followed by 40 cycles of denaturation at 95 °C for 30 sec, 95 °C for 5 sec, and 60 °C for 30 sec. The relative expression of mRNA was determined using the delta-delta CT method, and Gene expression was normalized to the expression of β-actin.

4.2.4 Establishing stable GS knockdown cells by lenti viral-induced shRNA

For establishing cell lines expressing shRNA against GS, four human unique shRNA lenti viral constructs (#1, #2, #3, and #4) (Sigma-Aldrich) were employed. For negative control, non-mammalian gene-targeting shRNA (NTC) was used. Lenti viruses were produced by co-transfecting HEK293T cells (ATCC) with each shRNA plasmid and 3rd generation packaging vectors (pMDLg/pRRE, pMD2.G-VSV-G, and pRSV-Rev) (Addgene) by using Lipofectamine 2000 (Invitrogen). The transfection media was replaced with fresh DMEM after 4 h of transfection. The incubated cell culture medium

containing viral particles was collected 48 h after transfection and passed through a 0.45 μm filter. The virus supernatant was then evenly distributed to cells (A2780, A549, and MOR cell lines) along with 4 μg/mL polybrene for cell line infection (Sigma-Aldrich). After 24 h, the virus supernatant was removed, and the cells were restored in the fresh culture medium. After 24 h, the medium was replaced with 2 μg/mL puromycin-containing medium, and pressure selection was performed on the basis of puromycin on packaged lentivirus vectors. Stable cell lines were cryopreserved after three generations of continuous passage and screening. Pools of four different shRNA sequences were used to target human GS: #1 (TRCN0000045631) 5'-CCAGGAGAAGAAGGGTTACTT-3'; #2 (TRCN0000343990) 5'-AGGAGAAGAAGGGTTACTTTG-3'; #3 (TRCN0000343992) 5'-CACACCTGTAAACGGATAATG-3'; #4 (TRCN0000344059) 5'-ATAACCACTGCTTCCATTTAA-3', and shNT.

4.2.5 Metabolite tracing analysis using CE-MS

Cells were seeded in six-well plates (8.8×10^5 cells in 2 mL medium) and cultured in a low glutamine medium (RPMI 1640, Sigma-Aldrich, Co. R0883 and DMEM, Nacalai, Co. 11584–85) with 10% FBS for overnight or the indicated time periods. For flux analysis, 1, 3, 6, and 12 h before sampling, the medium was replaced with a glutamine-free medium containing $^{13}C_5$-labeled glutamine (CLM-1822-H) with 10% dialyzed FBS.

The metabolite extraction method and CE-TOF/MS detection method are depicted above[120,121]. Data were analyzed by MasterHands[53].

4.2.6 Protein extraction and digestion

The cell samples were dissolved in 50 mM ammonium bicarbonate buffer containing 12 mM sodium deoxycholate (SDC), 12 mM sodium N-dodecanoylsarcosinate (SDDS), and 1% protease inhibitor (Protease Inhibitor Cocktail, Nacalai) and sonicated for 20 min using a Bioruptor II (BM Equipment). Protein concentration was measured using bicinchoninic acid (BCA) assay (Thermo), wherein 20 μg of protein was treated with dithiothreitol (DTT) for 30 min at 37 °C,

followed by iodoacetamide (IAM) for 30 min at 37 °C in the dark. After diluting with 50 mM ammonium carbonate five times, the samples were treated with Lys-C (Wako) for 3 h at 37 °C, followed by trypsin (Promega) (1:50 enzyme to protein ratio) overnight at 37 °C to digest proteins.

The peptides were desalted with an in-house tip containing a C18 disk (3M, Empore) and 10 mg C18 packing material (YMC GEL ODS-AQ)[122]. Each sample was dissolved in 0.1% formic acid (FA) and 2% acetonitrile after being concentrated and dried.

4.2.7 Quantitative Analysis with diaPASEF

The nano LC was performed on a nano HPLC system (nanoElute, Bruker), equipped with a hand-made spray needle column (75 μm i.d., 3 μm tip i.d., 250 mm length) packed with ACQUITY-BEH C18 material (1.7 μm, Waters). The mobile phase is composed of (A) 0.1% formic acid (FA) in water and (B) 0.1% FA in acetonitrile. The peptides were separated in 130 min at 280 nL/min using the following gradients: (A) + (B) = 100%, (B) 2%-35% (0–120 min), 35%-80% (120–125 min), 80%-80% (125‑130 min) under the column temperature of 60 °C.

Eluted peptides were analyzed on timsTOF Pro (Bruker Daltonics) in the Parallel Accumulation Serial Fragmentation-Data Dependent Acquisition (PASEF-DDA) mode to generate the spectral library[123]. Trapped Ion Mobility Spectrometry (TIMS) was enabled with a ramp time of 100 ms and a duty cycle of 100%. Ions with ion mobility from 0.6 to 1.6 V s/cm^2 were monitored. MS and MS/MS spectra were acquired from m/z 400 to 1200, and MS/MS data were acquired with 10 PASEF MS/MS scans per cycle. Isolation width was set to 2 m/z for m/z <700 and 3 m/z for m/z >800. Collision energy was increased stepwise from 20 to 59 eV as a function of increasing ion mobility from 0.6 to 1.6 V s/cm^2. In the Data Independent Acquisition (DIA) experiment, the MS was operated under the same conditions as in the DDA experiments except precursor selection. Precursor ions were selected using a diaPASEF acquitision scheme previously reported[124]. The LC-MS raw data and associated files were submitted to the ProteomeXchange Consortium via the jPOST partner repository (accession number: PXD041557) (accession number: JPST002115)[125].

4.2.8 Proteome data analysis

All LC-MS data were analyzed using PEAKS studio 10.6 (Bioinformatics Solutions)[126], and UniProt human protein database was used for protein identification. The error tolerance was set to 20 ppm for precursor ions and 0.05 Da for fragment ions; the enzyme was set to trypsin, and up to two missed cleavages were allowed. Carbamidomethylation at cysteine was set as a fixed modification. Protein N-terminal acetylation and oxidation at methionine were set as variable modifications, allowing for up to three positions per peptide. The identifications were filtered at a false discovery rate of 1% at peptide levels. The feature area of each identified peptide ion was calculated automatically with PEAKS software algorithm. The intensity-based quantification value of each identified protein was calculated from the feature area values.

The GO functional classification and annotations were obtained using the 'Wu Kong' platform (https://www.omicsolution.com/wkomics/main/)[127]. We used the Student's t-test for unpaired, two-tailed data to determine the statistical significance of FC in log2-transformed proteomic data. Pathway analysis was performed using Kyoto Encyclopedia of Genes and Genomes (KEGG) website (http://www.kegg.jp)[128].

4.3 Results

4.3.1 Knockdown of GS can effectively reduce the resistance of cells to platinum anticancer drugs

The GS expression levels of 609 cell lines from the expression atlas database (https://www.ebi.ac.uk/gxa/home)[129] were investigated, and human ovarian cancer A2780, non-small cell lung cancer A549, and MOR were used in the experiments. Ovarian cancer and non-small-cell lung carcinoma remain primarily treated with platinum-based drugs due to their initial effectiveness[76]. Although the three cell types display varying levels of GS expression, they all demonstrate resistance to platinum-based drugs, making them valuable models for studying drug resistance. In fact, A2780 belongs to a group of cell lines in the database that have relatively low GS

expression levels (Figure 4-1A). The GS expression level in A549 is 10 times that of A2780, and the GS expression level in MOR is 500 times that of A2780 (Figure 4-1A). RT-PCR confirmed that GS expression was significantly lower when compared to the negative control (Figure 4-1B). Our objective was to investigate the influence of different levels of GS expression on drug resistance following the inhibition of GS.

Subsequently, the sensitivities of GS-KD cells to platinum drugs were determined using an MTT assay (Figure 4-1C; Figure 4-1D). The vertical axis shows the cell viability 72 h after the addition of platinum drugs. It is noteworthy that the sensitivity of GS-KD cells is generally higher than that of control KD cells, i.e., resistance develops after GS knockdown, especially in #1 and #4. The resistance of the three cell lines to CDDP and carboplatin (CBDCA) before the knockdown of GS (refer to IC50) was not as different as the expression level of GS (Figure S2). Therefore, under the existing expression level of GS in cell lines, the inhibition of GS expression will reduce the sensitivity of cells to platinum drugs.

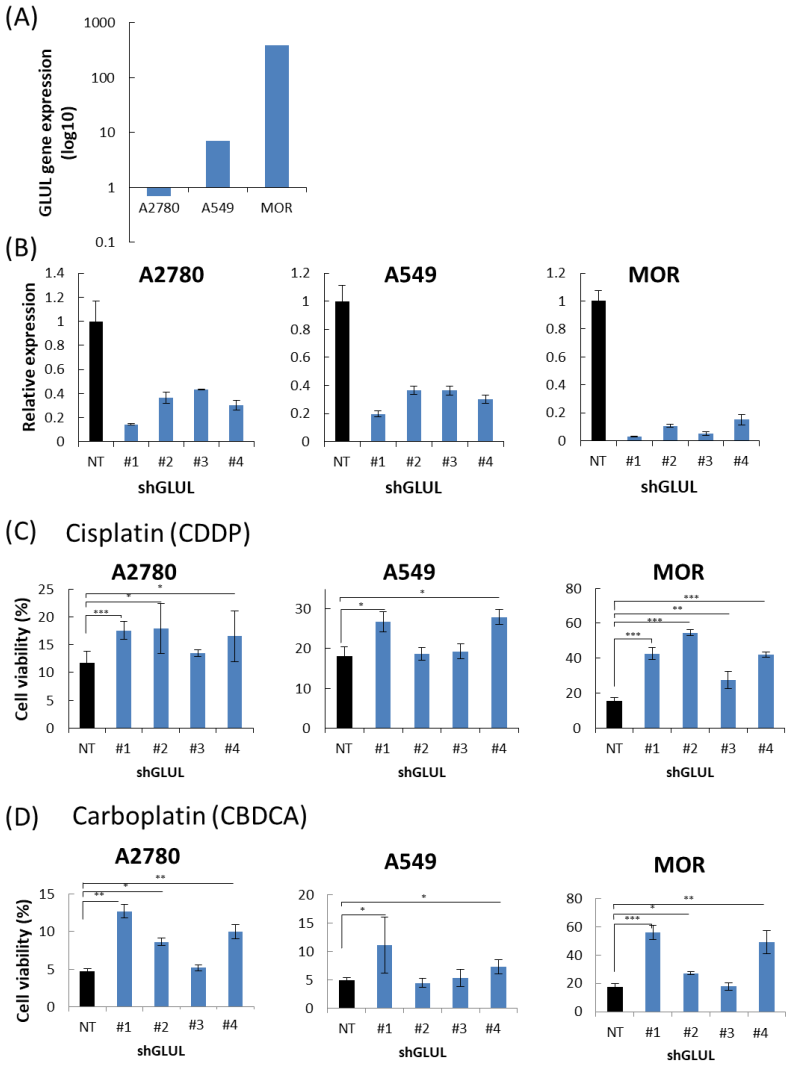

Figure 4-1 Inhibition of GS expression will reduce the sensitivity of cells to platinum drugs

(A) GLUL gene expression levels in A2780, A549, and MOR cell lines (Expression Atlas database). (B) The vertical axis shows the expression levels of GLUL detected by RT-PCR. Data are expressed as the mean ± standard deviation (SD) of three independent experiments. shRNA negative control (sh-NC, black bar) and si-GLUL (#1, #2, #3, and #4, blue bar) are shown with a horizontal line. (C, D) The negative control is represented by the black bar, and the viability of GS knockdown cell lines is represented by the blue bar. Cells were exposed to 16 μM (A2780 and A549) or 8 μM (MOR) of CDDP (C) or 128 μM (A2780 and MOR) or 256 μM (A549) of CBDCA (D), respectively. Cell viability was measured by MTT assay at 72 h after treatment. The relative percentage of untreated to control was calculated. The black bars represent sh-NC, while the blue bars represent sh-GLUL clones. Data are shown as mean value ±SD. Significance was determined using Student's t-test (*$p < 0.05$, **$p < 0.01$, ***$p < 0.001$).

4.3.2 GS knockdown led to a decrease in ferrochelatase in all three cell lines

Differential expression analysis of all quantified proteins was then performed to determine the effect of GS knockdown on the proteome of A2780, A549, and MOR cell lines. Negative control (NT) and five variants of #1, #2, #3, and #4 were obtained by shRNA for each of A2780, A549, and MOR cells, with three replicates per group; therefore, 15 samples were obtained for each cell type. Following preprocessing and missing value filtering using the k-Nearest Neighbors (kNN) algorithm (k = 5), A2780, A549, and MOR cells identified 6172, 5715, and 5433 quantifiable proteins, respectively[130]. Thresholds for significance were defined as an absolute fold change greater than 1.5 or less than 0.67 and a p-value of less than 0.05 by t-test (Figure S3). A2780 had 213 upregulated and 174 downregulated proteins; A549 had 142 upregulated and 114 downregulated proteins; MOR had 810 upregulated and 164 downregulated proteins. Among them, 42 upregulated proteins and 13 downregulated proteins were shared by more than two cell lines (Figure 4-2A; Figure 4-2B).

Among the three cell types, we observed a significant increase in the expression of two proteins. One of these proteins is Rab-like protein 6 (RABL6), which is known to be an oncogene associated with tumor development and may contribute to drug resistance in cancer. The other protein is oxygen-dependent coproporphyrinogen-III oxidase (CPOX), which serves as the sixth enzyme in the heme synthesis pathway (Figure 4-3A, B, C). Conversely, there was a notable decrease in the expression of ferrochelatase (FECH), an enzyme downstream of CPOX and the rate-limiting enzyme in the conversion of protoporphyrin to heme. Given these findings, we focused our attention on the heme synthesis pathway since two of the differentially expressed proteins among the three cell types are enzymes in this pathway. The upstream enzymes, such as CPOX, were more frequently expressed in the GS knockdown cell lines, whereas FECH expression was reduced (Figure 4-2A, B; Figure 4-3D, E). This observed pattern in enzyme expression suggests a potential accumulation of protoporphyrin and a reduction in heme synthesis when GS expression is inhibited. Overrepresentation analyses indicated that the upregulated common proteins were significantly associated with cancer-associated molecular pathways, such as the positive regulation of I-κB kinase/NF-κB signaling and innate immune response. In contrast,

drug-responsive proteins were downregulated in GS knockdown cell lines (Figure 4-2C; Figure 4-2D).

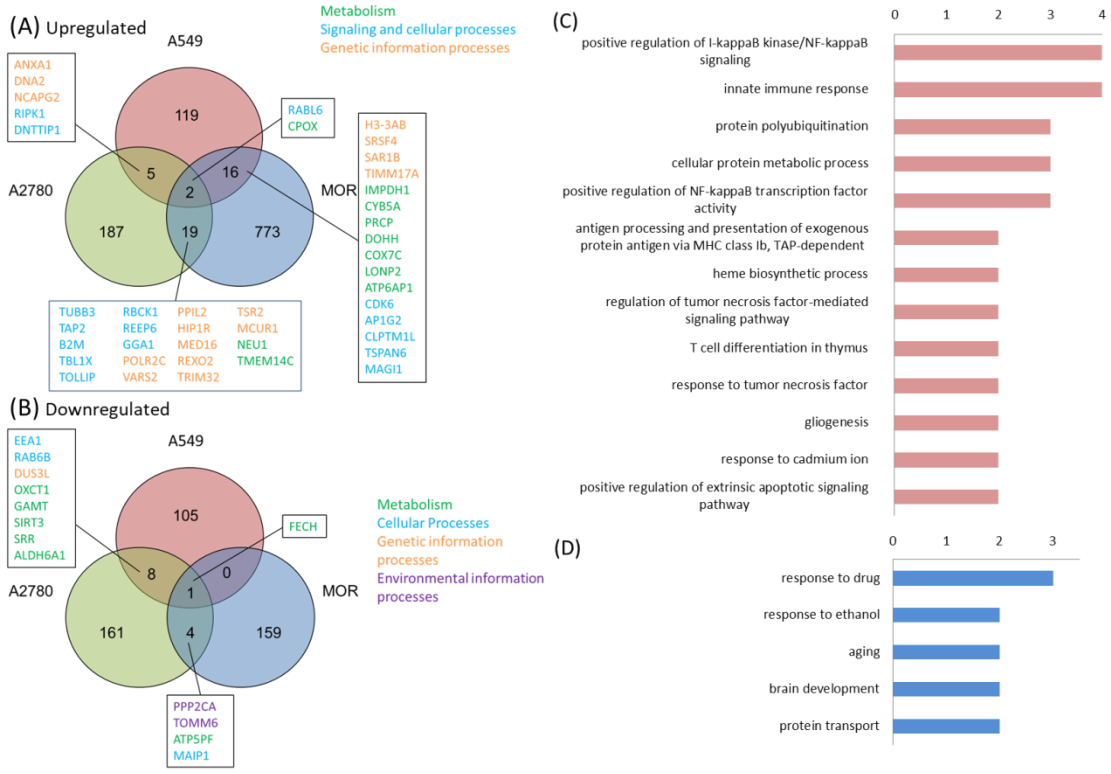

Figure 4-2 Differential expression analysis of proteomic data

(A) Venn diagram representing proteomics data of upregulated proteins among three cell lines. (B) Venn diagram representing proteomics data of downregulated proteins among three cell lines. (C) Bar graph representing overrepresentation analysis results of 42 upregulated proteins common to more than two cell lines by Gene Ontology (GO) biological process. The abscissa represents the number of enrichment factors (p.adjust < 0.005); the ordinate represents the enrichment items. (D) Bar graph representing overrepresentation analysis results of 13 downregulated proteins common to more than two cell lines by GO biological process. The condition was the same as in C.

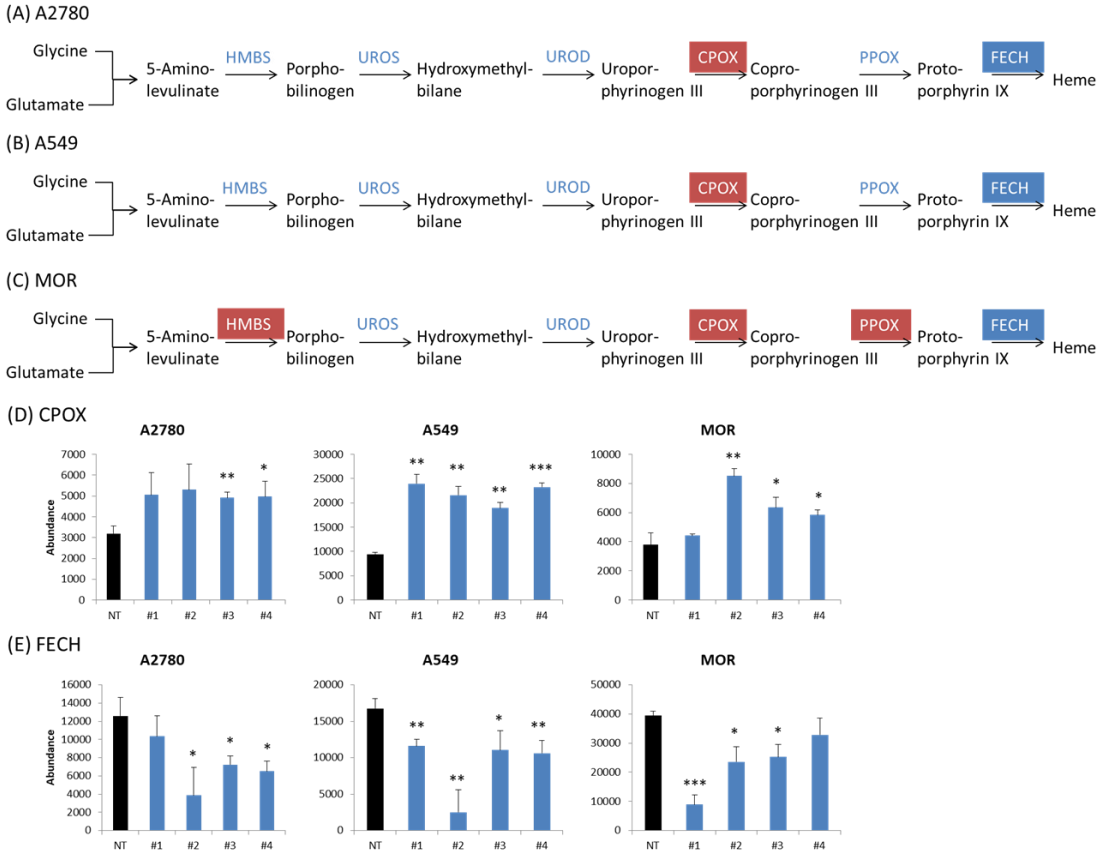

Figure 4-3 Expression of enzymes in heme biosynthesis pathway in cell lines

(A, B, C)The black texts indicate metabolites, the blue texts indicate the name of the gene corresponding to the metabolic enzyme, the red box represents upregulated enzyme, and the blue box represents downregulated enzyme. (D, E) The negative control is represented by the black bar, and the viability of GS knockdown cell lines is represented by the blue bar. The vertical axis represents protein abundance for CPOX and FECH. Data are shown as mean value +SD. Significance was determined using Student's t-test (*$p < 0.05$, **$p < 0.01$, ***$p < 0.001$).

4.3.3 Total glutathione increased after GS knockdown in all three cell lines

In ^{13}C flux experiment, negative control and four types of shGLUL in A2780, A549, and MOR cell lines were exposed to $^{13}C_5$-labeled glutamine for 1, 3, 6, and 12 h, and intracellular and extracellular metabolites were measured. To focus on the central carbon metabolites that contain the glutamine pathway, CE-TOF/MS was used for detection in positive and negative modes.

To evaluate the metabolic information of the different ^{13}C-glutamine fluxes, a pairwise comparison between GLUL knockdown groups and control groups was performed using orthogonal partial least squares discriminant analysis (OPLS-DA) (Figure 4-4). Q2Y were all higher than 0.5, indicating that the OPLS-DA model established in this study had goodness-of-fit and prediction ability (Figure 4-4A, B, C). The S-plot displays the detected metabolites, where the axis plotted from the prediction component was the covariance p[1] against the correlation p(corr)[1]. Metabolites with variable influence on projection (VIP) >1 strongly contributed to the observed differences among groups. Therefore, the red and blue dots in the figure are the differential substances of A2780, A549, and MOR cell lines (Figure 4-4D, E, F).

Metabolites were selected according to the criterion of VIP >1 and p-value <0.05, which differed between control and shGLUL groups of three cell lines by OPLS-DA analysis (Table 4-1, 2, 3). In A2780, gamma-aminobutyric acid (GABA) was significantly upregulated, whereas cysteine (Cys) and glycine (Gly), two amino acids involved in GSH synthesis, were significantly changed (Table 4-1). A549 cells showed significant changes in glutamate metabolism and GSH metabolism pathways (Table 4–2). A significant decrease was seen in MOR cells in the number of isotope-labeled glutamines (+01 ~ +05). This indicated that glutamine synthesis was downregulated. In addition, metabolites from the urea cycle, TCA cycle, and arginine metabolic pathway were found to be significantly downregulated in MOR cells (Table 4–3).

Figure 4–5 illustrates changes in glutamine-related metabolic pathways resulting from a comprehensive analysis of proteomics and metabolomics profiling of the GS knockdown in A2780, A549, and MOR cell lines. Enzymes involved in purine and pyrimidine metabolic pathways responsible for nucleotide degradation to nucleosides were upregulated in MOR cells after GLUL knockdown, while they were

downregulated in A549 and A2780 cells. Additionally, GSH levels increased significantly in A549 and MOR cells, while the oxidized state of GSSG was elevated in A2780 cells, likely due to an increase in glutathione peroxidase (Figure 4-5A, B, C; Figure 4-6 A, B).

However, the metabolic responses of these three cells differed considerably, making it challenging to identify any significant similarities. This is most likely because the basal expression levels of GS in the three cells varied greatly. In particular, the metabolic response of MOR cells was very different from that of the other cells.

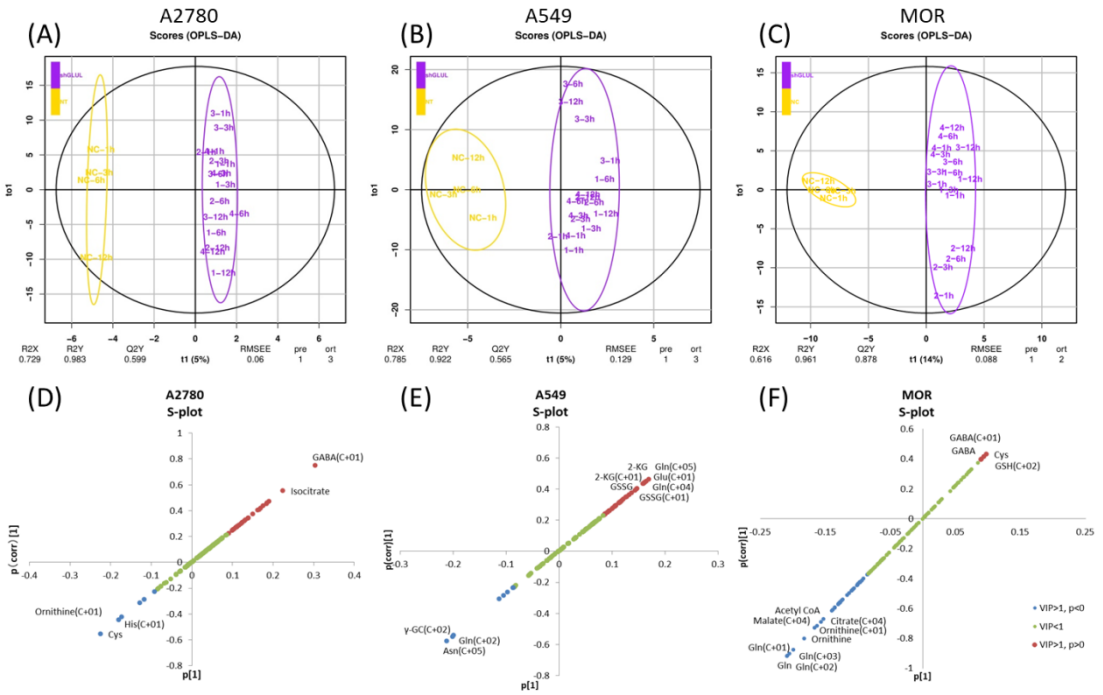

Figure 4-4 Differential expression analysis of metabolic data

(A, B, C) Score plot in the OPLS-DA model. In the score plot, the yellow text represents negative control, the purple text represents the shGLUL sample. 1, 3, 6, and 12 h represent the duration of isotope labeling. (D, E, F) In S-plot, the dot represents each individual metabolite or isotope-labeled metabolite. The farther a dot departs from the X and Y axes, the more the contribution to shGLUL samples and negative control. Among them, metabolites with VIP greater than 1 were considered crucial. VIP, a crucial variable, is a projection. Red dots in the S-plot represent the metabolites with VIP greater than 1 and increased in shGLUL samples, and blue dots represent the metabolites with VIP greater than 1 and reduced in shGLUL samples. Where R2X and R2Y, respectively, represent the percentages of X and Y matrix information explained by the PLS-DA model, whereas Q2Y is calculated through cross-validation to evaluate the prediction ability of the model. The larger the Q2Y, the better the prediction effect of the model.

Table 4-1 Metabolites that significantly change in shGLUL A2780

ID	p-value	VIP	change
GABA(+01)	0.000144	3.181984	increase
Cys	0.008948	2.716405	decrease
Isocitrate	0.014288	2.810726	increase
GABA	0.024424	2.072594	increase
His(+01)	0.041861	1.794719	decrease
Gly	0.049798	1.959492	increase

Table 4-2 Metabolites that significantly change in shGLUL A549

ID	p-value	VIP	change
Gln(+02)	0.017336	2.296228	increase
Asn(+05)	0.02089	2.228786	decrease
Gln(+05)	0.041441	2.104193	increase
gamma-Glu-cys(+02)	0.041861	1.982619	decrease
2-Oxoglutarate	0.049678	1.518982	increase

Table 4-3 Metabolites that significantly change in shGLUL MOR

ID	p-value	VIP	change
Gln	1.34E-08	2.454	decrease
Gln(+02)	2.19E-08	2.450	decrease
Gln(+03)	1.78E-07	2.411	decrease
Gln(+01)	7.58E-07	2.339	decrease
Ornithine	1.85E-05	2.140	decrease
Citrate(+04)	1.03E-04	1.913	decrease
Ornithine(+01)	2.55E-04	1.952	decrease
Acetyl CoA	0.001	1.792	decrease
Malate(+04)	0.002	1.842	decrease
cis-Aconitate(+04)	0.003	1.509	decrease
Arg(+01)	0.005	1.591	decrease
Fumarate(+04)	0.007	1.643	decrease
Arg	0.007	1.532	decrease
Citrate(+05)	0.008	1.627	decrease
Arg(+02)	0.010	1.494	decrease
Citrate(+03)	0.010	1.443	decrease

ID	p-value	VIP	change
Urea	0.010	1.587	decrease
Thr	0.013	1.524	decrease
Thr(+01)	0.014	1.493	decrease
Gln(+04)	0.017	1.503	decrease
Gln(+05)	0.021	1.463	decrease
Lys	0.028	1.366	decrease
Citrate(+02)	0.030	1.143	decrease
Asn	0.031	1.288	decrease
cis-Aconitate(+03)	0.034	1.102	decrease
Asn(+01)	0.034	1.243	decrease
Lactate(+03)	0.036	1.069	decrease
cis-Aconitate(+05)	0.038	1.289	decrease
Ser(+02)	0.042	1.332	decrease
Fumarate(+02)	0.045	1.169	decrease
Malate(+02)	0.046	1.180	decrease
His(+02)	0.050	1.131	decrease

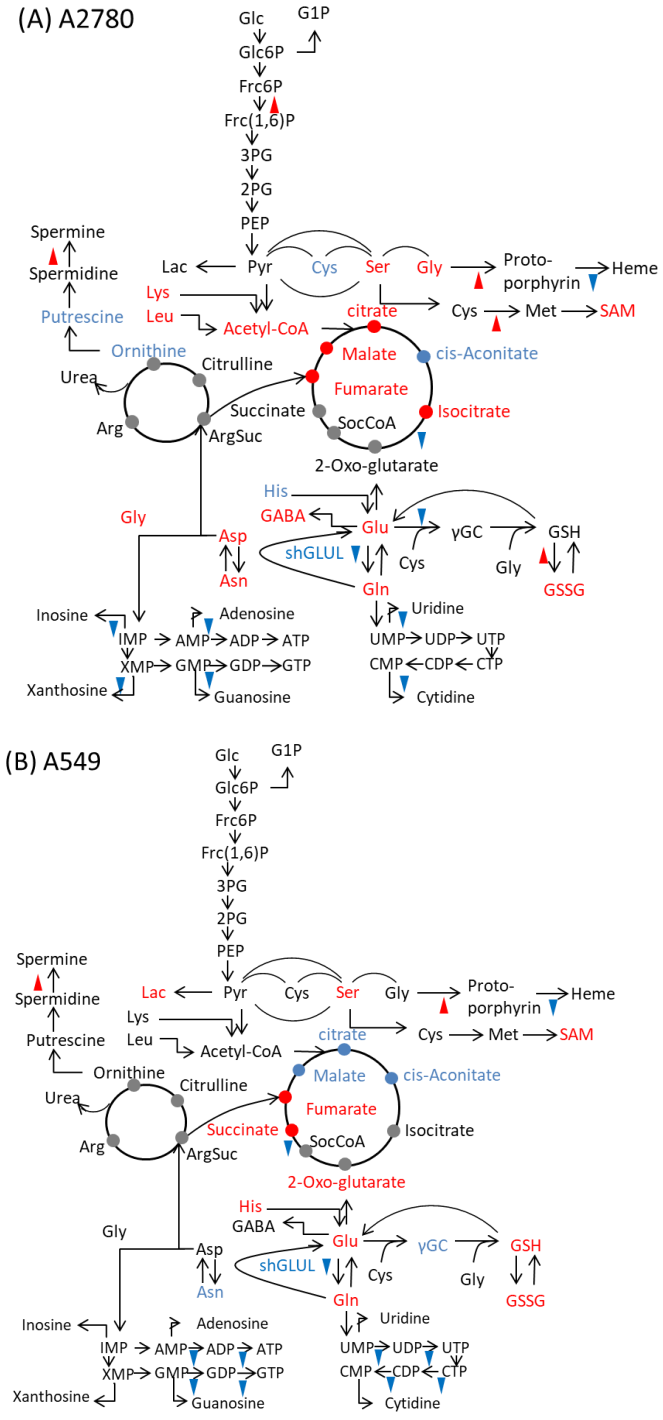
(A) A2780
Glc
G1P
Glc6P
Frc6P
Frc(1,6)P
3PG
2PG
PEP
Spermine
Spermidine
Putrescine
Ornithine
Urea
Arg
Lac
Pyr
Cys
Ser
Gly
Proto-
porphyrin
Heme
Lys
Leu
Acetyl-CoA
citrate
Cys
Met
SAM
Malate
cis-Aconitate
Fumarate
Citrulline
Succinate
SocCoA
Isocitrate
ArgSuc
2-Oxo-glutarate
His
GABA
Glu
γGC
GSH
Gly
Asp
Asn
shGLUL
Cys
Gly
GSSG
Gln
Inosine
Adenosine
Uridine
IMP
AMP
ADP
ATP
UMP
UDP
UTP
XMP
GMP
GDP
GTP
CMP
CDP
CTP
Xanthosine
Guanosine
Cytidine
(B) A549
Glc
G1P
Glc6P
Frc6P
Frc(1,6)P
3PG
2PG
PEP
Spermine
Spermidine
Putrescine
Ornithine
Urea
Arg
Lac
Pyr
Cys
Ser
Gly
Proto-
porphyrin
Heme
Lys
Leu
Acetyl-CoA
citrate
Cys
Met
SAM
Malate
cis-Aconitate
Fumarate
Citrulline
Succinate
SocCoA
Isocitrate
ArgSuc
2-Oxo-glutarate
His
GABA
Glu
γGC
GSH
Gly
Asp
Asn
shGLUL
Cys
Gly
GSSG
Gln
Inosine
Adenosine
Uridine
IMP
AMP
ADP
ATP
UMP
UDP
UTP
XMP
GMP
GDP
GTP
CMP
CDP
CTP
Xanthosine
Guanosine
Cytidine

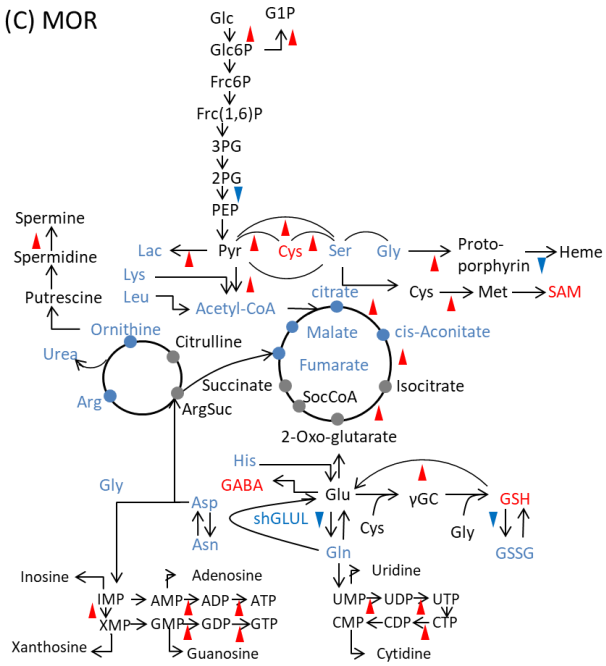

Figure 4-5 Differences in the expression of metabolites and enzymes in central carbon metabolism pathways

(A, B, C) Metabolic profiles of A2780, A549 and MOR cell lines, respectively. The red and blue texts indicate the increase and decrease of metabolites, respectively. The red triangle pointing up represents the upregulated enzymes and the blue triangle pointing down represents the downregulated enzymes.

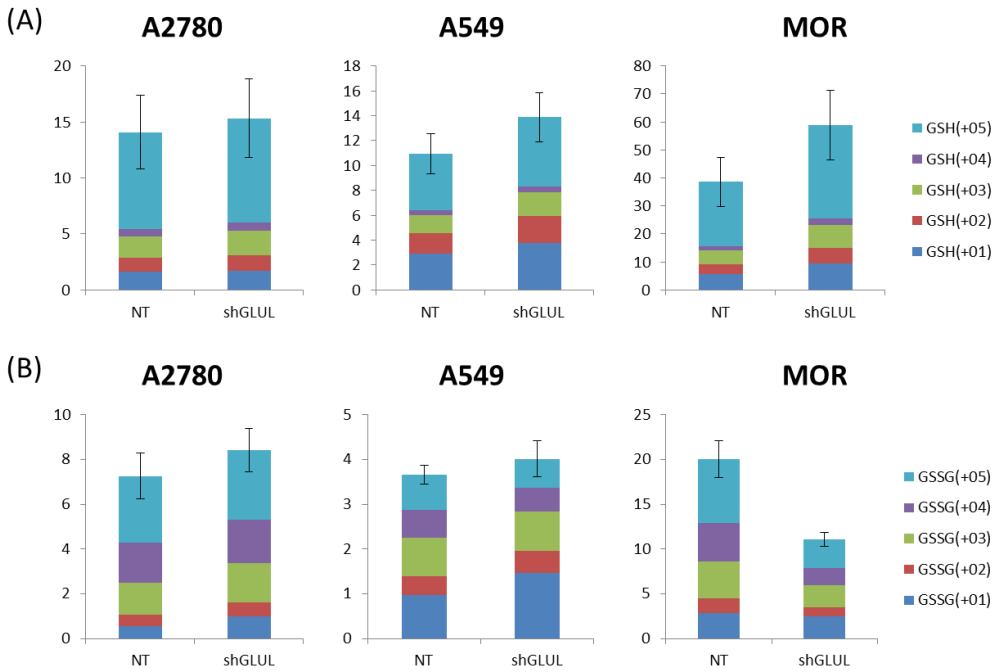

Figure 4-6 Glutathione levels increased slightly after GS knockdown in all three cell lines

(A, B) Cells were incubated with medium containing glutamine isotopically labeled at all five carbon atoms ($^{13}C_5$-glutamine) for 1 h, 3 h, 6 h and 12 h. Carbon fluxes from glutamine to GSH and GSSG were the sum of all time periods, shGLUL was the average of # 1 ~ # 4. Each bar color corresponds to the number of ^{13}C replaced with ^{12}C in the metabolites.

4.4 Discussion

In previous studies, high GS expression was linked to cancer cell proliferation and a poor prognosis, so inhibiting GS expression has been proposed as a possible treatment for cancer[83,119,131]. For example Ye et al. and Furusawa et al. successfully inhibited the growth of gastric and ovarian cancer tumors in mice by inhibiting glutamine transporters ASCT2 and GS[93,132]. However, limited research has been conducted on GS as a potential target for glutamine metabolism cancer therapy. This is mainly attributed to studies that have highlighted potential concerns associated with GS inhibition, including resistance to multiple anticancer drugs with diverse mechanisms or heightened inflammatory responses[93,110,112]. Nonetheless, our initial hypothesis in investigating GS was based on its potential versatility and significant impact on metabolism and signaling pathways.

The results of Chapter 3.1 revealed that GS knockdown increased resistance to anticancer drugs (Figure 4-1). Proteomic analysis revealed that GS knockdown activated the NF-κB pathway and the immune response, whereas drug response was inhibited (Figure 4-2C; Figure 4-2D). These findings suggested that GS was downregulated in cancer cells, making them more aggressive and resistant to anticancer drugs.

The proteomic analysis revealed interesting findings in the GS knockdown cell lines. Specifically, we observed a consistent increase in CPOX levels, along with a uniform decrease in FECH levels within the heme biosynthesis pathways (Figure 4-2A, B; Figure 4-A, B, C). These changes indicated an upregulation of the porphyrin metabolism pathway, leading to the accumulation of porphyrins, while the downregulation of FECH, a key enzyme in heme synthesis, potentially resulted in a reduction in heme production. It has been reported that inhibiting FECH can cause iron overload in lysosomes, subsequently enhancing oxidative stress and triggering lipid peroxidation, ultimately leading to ferroptosis[133]. Moreover, previous studies have linked ferroptosis to mitochondrial glutaminase (GLS2) and cystine/glutamate transporter (SLC7A11)[134,135], both of which are metabolically associated with GS. Building upon these findings, our results suggest that GS may exert a positive influence on ferroptosis through the regulation of FECH in cancer cells. However, further experimental investigations and

measurements are required to validate this hypothesis. While GS generally promotes cell proliferation, it may also induce cell death through mechanisms such as FECH regulation.

What GS does to promote cancer cell growth has been shown to activate the P38 MAPK signaling pathway and increase purine nucleotide synthesis[136-138]. Glutamine provides amide and amino nitrogen for purine and pyrimidine synthesis, and each shGLUL cell line can influence the activities of purine and pyrimidine metabolism enzymes[139]. However, their manifestations vary for each cell line. According to Figure 4-5, enzyme expression in the purine and pyrimidine metabolic pathways was upregulated in MOR cells following GLUL knockdown whereas it was downregulated in A549 and A2780 cells. We hypothesized that this was due to a large difference in the basal expression of GS, for example, MOR cells had 500 times more GS expression than A2780 cells.

Interestingly, we observed similarities in the glutamine pathways among these three cell lines. As depicted in Figure 4-6, the total production of GSH or its oxidized form GSSG increased when GS was knocked down. GSH plays a crucial role as a key component of the cellular antioxidant defense system against ROS and electrophiles. Firstly, it has been established that GSH can enhance drug resistance in cancer cells[140]. Secondly, recent studies have indicated a connection between glutathione metabolism and ferroptosis[141]. Cao et al. demonstrated that the sensitivity of cells to glutathione-dependent ferroptosis is influenced by the total glutathione levels and the maintenance of intracellular GSH, which partially protects cells from the impact of ferroptosis[142]. Notably, the elevated levels of total glutathione and inhibition of heme synthesis, as observed in our study, suggest a potential direction of GS inhibition towards reducing vulnerability to ferroptosis. However, further research is necessary to establish a definitive association between ferroptosis and GS.

4.5 Conclusions

Despite its controversial role, GS is not currently recognized as a cancer biomarker. While it can act as a nutritional supplement in cases where glutamine is required, inhibiting GS has been shown to halt the growth of cancer cells. However, recent investigations have gradually revealed an association between GS and cancer drug resistance. Our study suggests that GS affects a wide range of metabolic pathways,

including the heme synthesis pathway, the glutamine pathway, and the purine and pyrimidine pathways. Additionally, it may also be linked to ferroptosis. Perturbations in these metabolic pathways may contribute to cancer drug resistance and initiate other functions that hinder effective cancer therapy. Consequently, we believe that GS has the potential to serve as a crucial monitoring target for evaluating malignancy levels and trends in disease progression.

Chapter 5 Concluding remarks

This article presents several studies exploring the applications of metabolomics and proteomics analyses in evaluating the biological effects of drugs, including chemotherapeutic agents and traditional herbal medicines. Metabolomics focuses on the analysis of small molecules and is highly valuable in understanding candidate drugs and aiding target selection. Central carbon metabolism serves as the primary energy source and precursor for other metabolic pathways, making it crucial in all living organisms. Therefore, the study of metabolite expression related to central carbon metabolism and amino acid metabolism holds significant importance. CE-MS was employed in this research as it enables the simultaneous qualitative and quantitative characterization of most substances within the central carbon metabolic pathway.

In Chapter 2, a comprehensive evaluation of 416 polar small-molecule metabolites from 30 Chinese medicinal materials was performed using CE-MS-based metabolomics. The study aimed to analyze the molecular-level aspects of the "Four-nature" principle, a fundamental concept in TCM. Among more than half of the Chinese herbal medicines, 193 compounds were identified, and the concentrations of 5-dihydroxybenzoate, 2-hydroxyvalerate, N-acetylglucosamine, and uracil were significantly higher in cold herbs compared to hot herbs ($p < 0.01$). In contrast, L-glutamine concentration was significantly higher in hot herbs than in cold herbs ($p < 0.01$). PCA revealed a stronger association between amino acid content and cold herbs. The Tanimoto coefficient was then used to calculate the similarity between the detected compounds, followed by cluster analysis to group similar molecules and compare their contents. The findings indicated that nucleoside metabolites tended to be more abundant in hot herbs. Extracellular nucleosides have previously been associated with immunity and inflammation. The work of Liang et al. suggests a correlation between hot-nature herbs and the regulation of inflammation and immunity through pathways such as MAPK, TNF, IL8, TLR, and HTR[69]. In addition, hot herbs had a higher frequency of purine-like chemical fragments, particularly those with a double-ring structure [69]. This suggests that hot herbs may promote immune and inflammatory regulation through nucleoside analogs. It is important to note that the different energetic properties of hot, warm, cold,

and cool herbs are not solely determined by a single chemical molecule or class, but rather by the combined action of all components, known as molecular groups[143].

Understanding the mechanisms of drug resistance is crucial to overcome one of the major challenges in chemotherapy. In Chapter 3, the study focused on detecting qualitative and quantitative information on 189 metabolites in CDDP-sensitive ovarian cancer A2780 cells and CDDP-resistant A2780cis cells. The results revealed significantly increased levels of glutamine, glutamate, and GSH in A2780cis cells. Therefore, the study emphasizes the importance of glutamine metabolism in drug resistance. Cell experiments further confirmed that both glutamine starvation and hindrance could reduce GSH levels and CDDP resistance in A2780cis cells. Interestingly, GS expression was completely inhibited in A2780cis cells. Increasing GS expression through the use of 5-Aza-dC resulted in decreased CDDP resistance, while GS knockdown using siRNA techniques increased CDDP resistance. Taken together, these results suggest a model in which suppressed GS expression in resistant cells leads to high levels of GSH, while levels of TCA cycle metabolites are reduced compared to sensitive cells. Therefore, the study suggests that GS expression may be one of the factors to monitor the development of CDDP resistance. Previous studies have indicated that CG island methylation and gene silencing are associated with CDDP resistance in ovarian cancer cell lines. In a study by Li et al. significant changes in DNA methyltransferase proteins of A2780 resistant cell lines were observed, indicating the inhibitory effects of methylation on many factors[144]. Therefore, in addition to GS, several other factors influence CDDP resistance in A2780cis cells.

In Chapter 3, the study highlights the role of GS and glutamine metabolism in influencing CDDP resistance in ovarian cancer cell lines. Consequently, Chapter 4 aimed to investigate the functional aspects of GS by constructing human ovarian cancer A2780 cells, small-cell carcinoma A549 cells, and MOR cell lines with GS inhibited by shRNA. Knockdown of GS resulted in decreased resistance to platinum drugs in all three cell lines, validating the findings of Chapter 3. Metabolomic analysis revealed distinct glutamine metabolism trends upon GS knockdown in the three cell types. At the proteomic level, downregulation of GS activated the NF-κB pathway and the immune response, while inhibiting the cell response to drugs. In the shGS cell line, all three cell lines showed upregulation of CPOX and downregulation of FECH in the porphyrin

metabolic pathway. FECH acts as a rate-limiting enzyme involved in the conversion of protoporphyrin to heme, and GS knockdown resulted in reduced FECH expression which is believed to hinder heme synthesis [145]. At the metabolomic level, GS knockdown showed different trends in purine and pyrimidine metabolism in the three cell lines, although all three cell lines showed upregulation of GSH synthesis. Ferroptosis, an alternative apoptotic process, is characterized by glutathione depletion and release of free iron from heme. Evidence suggests that inhibition of GS promotes GSH production and decreases heme production, potentially leading to a reduction in ferroptosis[146]. However, the relationship between GS and ferroptosis requires further investigation. For example, measuring the extent of lipid peroxidation after GS knockdown may provide additional evidence in this regard.

Chapter 2 of this research contributes novel perspectives to the existing literature on the "hot and cold-natured" categorization in TCM. The study not only verifies the feasibility of using CE-TOF/MS to detect metabolites in herbal medicine, but also developed a method to analyze herbal metabolites by comparing molecular similarity and MS quantitative data. From our understanding, this is the first study to combine molecule fragments and mass spectrometry quantification to study herbal medicine. Small-molecule drugs have a long history of development, and plants have been a treasure trove for the discovery of such drugs, while some low-weight molecules less than 300 daltons have the advantage of high binding efficiency, although their pharmacological activity may be weak. In modern small-molecule drug discovery, the fragment-based drug discovery approach refers to the discovery and development of new drugs by screening small-molecule fragments with weak interactions with target proteins using nuclear magnetic resonance, surface plasmon resonance, and X-ray single crystal diffraction analysis, and later optimizing the active fragments based on their structural information. The development of new small-molecule drugs can benefit from the use of CE-TOF/MS to investigate the efficacy of traditional Chinese herbal remedies at the molecular level.

Even though drug resistance has been widely studied, the present study identified new targets for resistance inhibition from a metabolic perspective. In Chapter 3, it confirms GS as a regulator of CDDP resistance in ovarian cancer cell lines, which opens a way for future research to consider the solution of drug resistance by metabolic

inhibitors. GS, known as a rate-limiting enzyme in glutamine synthesis, has predominantly been viewed as a potential target for cancer therapy. However, our study highlights some negative implications associated with GS. Chapter 4 focuses on the functional analysis of GS using proteomics and metabolomics approaches. The results show that the association between GS and drug resistance is consistent across different species of cancer cell lines. Moreover, the study reveals potential negative consequences, such as the inhibition of ferroptosis in cancer cells. Preclinical research has a risk component that focuses primarily on the mechanism of action of the drug. The discovery of pharmacological targets will have a significant impact on the longevity of the drug if it underestimates the biological complexity or ignores the pleiotropic nature of the targets. Clarity of the upstream and downstream pathways of the target is critical for the development of novel drugs targeting metabolic enzymes. Therefore, metabolomics and proteomics methods are very useful for elucidating the mechanism of drug action and exploring drug targets, and may be suitable for multi-factorial personalized medical applications in the future.

Acknowledgements

First and foremost, I would like to salute Professor Masaru Tomita, who established the Institute for Advanced Biosciences (IAB) Keio University, and Professor Tomoyoshi Soga, who established the unique CE-MS platform here. Professor Tomita's course at the Shonan Fujisawa Campus introduced me to the life sciences and to the Tsuruoka Campus, where I spent more than six years. Here I met Professor Soga and was introduced to his mass spectrometry technology, which will help me in my future studies and career development. Thank you very much for the innovative study atmosphere and the tremendous support you provided throughout.

Keiko Iino, Dr. Masahiro Sugimoto and Dr. Mitsuhiro Kitagawa provided invaluable assistance in my study on Chinese herbal medicine in Chapter 2. When I first started in the seminar, I was fortunate to have a very considerate individual like Iino as my academic advisor, she and Dr. Kitagawa taught me a lot about the project.

I would like to convey my heartfelt gratitude to Dr. Masaru Mori, Dr. Sho Tabata, Dr. Kiyotoshi Satoh, and Dr. Shojiro Kitajima for their assistance in the studying Chapters 3 and 4. Dr Tabata has provided much guidance in previous experiments, and Dr Mori has been a great help and guide in proteomics. Dr. Satoh helped me diligently rewrite my manuscript until publication, in addition to the experimental guidance; Dr. Kitajima also provided a lot of experimental advice late in the study. It would be extremely difficult to complete the study without their invaluable help.

Furthermore, I would like to thank Dr. Akiyoshi Hirayama and Ms. Kaori Igarashi of the Metabolome Group for their continuous assistance with MS detection and data processing. And many thanks to Professor Akio Kanai, Professor Kazuharu Arakawa and Professor Yasuhiro Naito for their encouragement and direction. My colleagues in the same lab, Megumi Uetaki and Ryosuke Hayasaka, have been extremely supportive and tolerant.

Many thanks to the Taikichiro Mori Memorial Study Grant for supporting the study. And Lotte Foundation for helping me to live and study.

Finally, I would like to thank my family for their encouragement and support. They are the ones who motivate me to keep going.

References

1. Voit, E. O. Perspective: Dimensions of the scientific method. *PLoS Comput. Biol.* **15**, e1007279 (2019).
2. Wörheide, M. A., Krumsiek, J., Kastenmüller, G. & Arnold, M. Multi-omics integration in biomedical research – A metabolomics-centric review. *Anal. Chim. Acta* **1141**, 144–162 (2021).
3. Maretty, L. *et al.* Sequencing and de novo assembly of 150 genomes from Denmark as a population reference. *Nature* **548**, 87–91 (2017).
4. Griffith, M., Walker, J. R., Spies, N. C., Ainscough, B. J. & Griffith, O. L. Informatics for RNA Sequencing: A Web Resource for Analysis on the Cloud. *PLoS Comput. Biol.* **11**, 1–20 (2015).
5. Aslam, B., Basit, M., Nisar, M. A., Khurshid, M. & Rasool, M. H. Proteomics: Technologies and their applications. *J. Chromatogr. Sci.* **55**, 182–196 (2017).
6. Fiehn, O. Metabolomics-the link between genotypes and phenotypes. *Plant Mol. Biol.* **48**, 155–171 (2002).
7. Bujak, R., Struck-Lewicka, W., Markuszewski, M. J. & Kaliszan, R. Metabolomics for laboratory diagnostics. *J. Pharm. Biomed. Anal.* **113**, 108–120 (2015).
8. Wishart, D. S. Emerging applications of metabolomics in drug discovery and precision medicine. *Nat. Rev. Drug Discov.* **15**, 473–484 (2016).
9. Kroemer, G. & Pouyssegur, J. Tumor Cell Metabolism: Cancer's Achilles' Heel. *Cancer Cell* **13**, 472–482 (2008).
10. Kumar, A. & Misra, B. B. Challenges and Opportunities in Cancer Metabolomics. *Proteomics* **19**, e1900042 (2019).
11. Liang, L., Sun, F., Wang, H. & Hu, Z. Metabolomics, metabolic flux analysis and cancer pharmacology. *Pharmacol Ther.* **224**, 107827 (2021).
12. Jang, C., Chen, L. & Rabinowitz, J. D. Metabolomics and Isotope Tracing. *Cell* **173**, 822–837 (2018).
13. Luengo, A., Gui, D. Y. & Vander Heiden, M. G. Targeting Metabolism for Cancer Therapy. *Cell Chem. Biol.* **24**, 1161–1180 (2017).

14. Harvey, A. L., Edrada-Ebel, R. & Quinn, R. J. The re-emergence of natural products for drug discovery in the genomics era. *Nat. Rev. Drug Discov.* **14**, 111–129 (2015).

15. Newman, D. J. & Cragg, G. M. Natural Products as Sources of New Drugs over the Nearly Four Decades from 01/1981 to 09/2019. *J. Nat. Prod.* **83**, 770–803 (2020).

16. Zhu, Y. P. & Woerdenbag, H. J. Traditional Chinese herbal medicine. *Pharm. World Sci.* **17**, 103–112 (1995).

17. Xu, Q. *et al.* The quest for modernisation of traditional Chinese medicine. *BMC Complement. Altern. Med.* **13**, 132 (2013).

18. Wang, M. *et al.* Metabolomics in the context of systems biology: bridging traditional Chinese medicine and molecular pharmacology. *Phytother. Res.* **19**, 173–182 (2005).

19. Guo, R. *et al.* Omics strategies decipher therapeutic discoveries of traditional Chinese medicine against different diseases at multiple layers molecular-level. *Pharmacol. Res.* **152**, 104627 (2020).

20. Jang, S., Lee, A. & Hwang, Y. H. Chemical Profile Determination and Quantitative Analysis of Components in Oryeong-san Using UHPLC-Q-Orbitrap-MS and UPLC-TQ-MS/MS. *Molecules* **28**, 3685 (2023).

21. Wang, T., Liu, J., Luo, X., Hu, L. & Lu, H. Functional metabolomics innovates therapeutic discovery of traditional Chinese medicine derived functional compounds. *Pharmacol. Ther.* **224**, 107824 (2021).

22. Cao, H., Zhang, A., Zhang, H., Sun, H. & Wang, X. The application of metabolomics in traditional Chinese medicine opens up a dialogue between Chinese and Western medicine. *Phytother. Res.* **29**, 159–166 (2015).

23. Wang, M. *et al.* Metabolomics highlights pharmacological bioactivity and biochemical mechanism of traditional Chinese medicine. *Chem. Biol. Interact.* **273**, 133–141 (2017).

24. Wang, X.-J. *et al.* Novel applications of mass spectrometry-based metabolomics in herbal medicines and its active ingredients: Current evidence. *Mass Spectrom. Rev.* **38**, 380–402 (2019).

25. Wang, X. *et al.* Potential role of metabolomics apporoaches in the area of traditional Chinese medicine: As pillars of the bridge between Chinese and Western medicine. *J. Pharm. Biomed. Anal.* **55**, 859–868 (2011).

26. Zhang, A. *et al.* Metabolomics: towards understanding traditional Chinese medicine. *Planta Med.* **76**, 2026–2035 (2010).

27. Liu, Y., Beyer, A. & Aebersold, R. On the Dependency of Cellular Protein Levels on mRNA Abundance. *Cell* **165**, 535–550 (2016).

28. Uhlén, M. *et al.* Proteomics. Tissue-based map of the human proteome. *Science* **347**, 1260419 (2015).

29. Jiang, L. *et al.* A Quantitative Proteome Map of the Human Body. *Cell* **183**, 269–283 (2020).

30. Adhikari, S. *et al.* A high-stringency blueprint of the human proteome. *Nat.Commun.***11**, 1–16 (2020).

31. Jiang, Y. *et al.* Proteomics identifies new therapeutic targets of early-stage hepatocellular carcinoma. *Nature* **567**, 257–261 (2019).

32. Savino, R., Paduano, S., Preianò, M. & Terracciano, R. The proteomics big challenge for biomarkers and new drug-targets discovery. *Int. J. Mol. Sci.* **13**, 13926–13948 (2012).

33. Dias, M. H., Kitano, E. S., Zelanis, A. & Iwai, L. K. Proteomics and drug discovery in cancer. *Drug Discov. Today* **21**, 264–277 (2016).

34. Burbaum, J. & Tobal, G. M. Proteomics in drug discovery. *Curr. Opin. Chem. Biol.* **6**, 427–433 (2002).

35. Meissner, F., Geddes-McAlister, J., Mann, M. & Bantscheff, M. The emerging role of mass spectrometry-based proteomics in drug discovery. *Nat. Rev. Drug Discov.* **21**, 637–654 (2022).

36. Jiang, Y., David, B., Tu, P. & Barbin, Y. Recent analytical approaches in quality control of traditional Chinese medicines-A review. *Anal Chim Acta.* **657**, 9–18 (2010).

37. Jia, Y., Zhang, Z.-Z., Wei, Y.-H., Xue-Mei, Q. & Li, Z.-Y. Metabolomics coupled with similarity analysis advances the elucidation of the cold/hot properties of traditional Chinese medicines. *Chin. J. Nat. Med.* **15**, 631–640 (2017).

38. Khan, I. A. & Smillie, T. Implementing a 'quality by design' approach to assure the safety and integrity of botanical dietary supplements. *J. Nat. Prod.* **75**, 1665–1673 (2012).

39. Fu, J., Pang, J., Zhao, X. & Han, J. The Quantitative Ideas and Methods in Assessment of Four Properties of Chinese Medicinal Herbs. *Cell Biochem. Biophys.* **71**, 1307–1312 (2015).

40. Chan, K. Chinese medicinal materials and their interface with Western medical

concepts. *J. Ethnopharmacol.* **96**, 1–18 (2005).

41. Yuan, H. *et al.* How can synergism of traditional medicines benefit from network pharmacology? *Molecules* **22**, 1–19 (2017).

42. Zhou, X. *et al.* Synergistic effects of Chinese herbal medicine: A comprehensive review of methodology and current research. *Front. Pharmacol.* **7**, 1–16 (2016).

43. Yi, T. *et al.* Comparison of ten major constituents in seven types of processed tea using HPLC-DAD-MS followed by principal component and hierarchical cluster analysis. *LWT--Food Sci. Technol.* **62**, 194–201 (2015).

44. Iino, K., Sugimoto, M., Soga, T. & Tomita, M. Profiling of the charged metabolites of traditional herbal medicines using capillary electrophoresis time-of-flight mass spectrometry. *Metabolomics* **8**, 99–108 (2012).

45. Zhang, A., Sun, H. & Wang, X. Recent highlights of metabolomics for traditional Chinese medicine. *Pharmazie* **67**, 667–675 (2012).

46. Li, B., He, X., Jia, W. & Li, H. Novel Applications of Metabolomics in Personalized Medicine: A Mini-Review. *Molecules* **22**, 1–10 (2017).

47. Zhang, J. *et al.* Discriminant Analysis of Traditional Chinese Medicinal Properties Based on Holistic Chemical Profiling by 1H-NMR Spectrometry. *Evid. Based. Complement. Alternat. Med.* **2020**, 3141340 (2020).

48. Soga, T. *et al.* Quantitative Metabolome Analysis Using Capillary Electrophoresis Mass Spectrometry. *J. Proteome Res.* **2**, 488–494 (2003).

49. Soga, T. *et al.* Differential metabolomics reveals ophthalmic acid as an oxidative stress biomarker indicating hepatic glutathione consumption. *J. Biol. Chem.* **281**, 16768–16776 (2006).

50. Sato, S., Arita, M., Soga, T., Nishioka, T. & Tomita, M. Time-resolved metabolomics reveals metabolic modulation in rice foliage. *BMC Syst. Biol.* **2**, 1–13 (2008).

51. Ardekani, M. R. S., Rahimi, R., Javadi, B., Abdi, L. & Khanavi, M. Relationship between temperaments of medicinal plants and their major chemical compounds. *J Tradit Chin Med.* **31**, 27–31 (2011).

52. Fu, X. J. *et al.* Study on the networks of 'nature-Family-Component' of Chinese medicinal herbs based on association rules mining. *Chin. J. Integr. Med.* **19**, 663–667 (2013).

53. Sugimoto, M., Wong, D. T., Hirayama, A., Soga, T. & Tomita, M. Capillary

electrophoresis mass spectrometry-based saliva metabolomics identified oral, breast and pancreatic cancer-specific profiles. *Metabolomics* **6**, 78–95 (2010).

54. Sugimoto, M. *et al.* Metabolomic profiles and sensory attributes of edamame under various storage duration and temperature conditions. *J. Agric. Food Chem.* **58**, 8418–8425 (2010).

55. Saeed, A. I. *et al.* TM4: a free, open-source system for microarray data management and analysis. *Biotechniques* **34**, 374–378 (2003).

56. Kim, S. *et al.* PubChem substance and compound databases. *Nucleic Acids Res.* **44**, D1202–D1213 (2016).

57. Rogers, D. J. & Tanimoto, T. T. A Computer Program for Classifying Plants. *Science* **132**, 1115–1118 (1960).

58. O'Boyle, N. M. *et al.* Open Babel: An open chemical toolbox Noel. *J. Cheminform.* **3**, 1–14 (2011).

59. Mar, J. C., Wells, C. A. & Quackenbush, J. Defining an informativeness metric for clustering gene expression data. *Bioinformatics* **27**, 1094–1100 (2011).

60. Zeng, W. B. *et al.* Distribution of nucleosides in populations of Cordyceps cicadae. *Molecules* **19**, 6123–6141 (2014).

61. Ou, B., Huang, D., Hampsch-Woodill, M. & Flanagan, J. A. When east meets west: the relationship between yin-yang and antioxidation-oxidation. *FASEB J.* **17**, 127–129 (2003).

62. Liao, H., Banbury, L. K. & Leach, D. N. Antioxidant activity of 45 Chinese herbs and the relationship with their TCM characteristics. *J. Evidence-Based Complement. Altern. Med.* **5**, 429–434 (2008).

63. Hou, Z. K. *et al.* Reviews and Thoughts on the Relevance between Qualitative Chinese Medicinal Properties and Quantitative Material Components. *J. Evidence-Based Complement. Altern. Med.* **2020**, 2020: 8643746 (2020).

64. Liang, S. On Macroscopic Chemical Components of Four Properties and Five Tastes of Chinese Materia Medica. *Shanghai J. Tradit. Chinese Med.* **42**, 63–67 (2008).

65. Hill, B. G., Shiva, S., Ballinger, S., Zhang, J. & Darley-Usmar, V. M. Bioenergetics and translational metabolism: implications for genetics, physiology and precision medicine. *Biol. Chem.* **401**, 3–29 (2019).

66. Giuliani, A. L., Sarti, A. C. & Di Virgilio, F. Extracellular nucleotides and nucleosides

as signalling molecules. *Immunol. Lett.* **205**, 16–24 (2019).

67. Chattopadhyay, D. *et al.* Recent advancements for the evaluation of anti-viral activities of natural products. *N. Biotechnol.* **25**, 347–368 (2009).

68. Guinan, M., Benckendorff, C., Smith, M. & Miller, G. J. Recent Advances in the Chemical Synthesis and Evaluation of Anticancer Nucleoside Analogues. Molecules **25**, 1869–1883 (2020).

69. Liang, F. *et al.* Molecular network and chemical fragment-based characteristics of medicinal herbs with cold and hot properties from Chinese medicine. *J. Ethnopharmacol.* **148**, 770–779 (2013).

70. Roseberg, B., Vancamp, L. & Krigas, T. Inhibition of cell division in escherichia coli by electrolysis products from a platinum electrode. *Nature* **205**, 698–699 (1965).

71. Lebwohl, D. & Canetta, R. Clinical development of platinum complexes in cancer therapy: an historical perspective and an update. *Eur. J. Cancer* **34**, 1522–1534 (1998).

72. Galluzzi, L. *et al.* Molecular mechanisms of cisplatin resistance. *Oncogene* **31**, 1869–1883 (2012).

73. Jamieson, E. R. & Lippard, S. J. Structure, recognition, and processing of cisplatin-DNA adducts. *Chem. Rev.* **99**, 2467–2498 (1999).

74. Wang, D. & Lippard, S. J. Cellular processing of platinum anticancer drugs. *Nat.Rev.Drug Discov.* **4**, 307–320 (2005).

75. Reedijk, J. Why does cisplatin reach guanine-n7 with competing s-donor ligands available in the cell? *Chem. Rev.* **99**, 2499–2510 (1999).

76. Dasari, S. & Bernard Tchounwou, P. Cisplatin in cancer therapy: Molecular mechanisms of action. *Eur. J. Pharmacol.* **740**, 364–378 (2014).

77. Winter, W. E. *et al.* Tumor residual after surgical cytoreduction in prediction of clinical outcome in stage IV epithelial ovarian cancer: A Gynecologic Oncology Group study. *J. Clin. Oncol.* **26**, 83–89 (2008).

78. Oronsky, B. *et al.* A brief review of the management of platinum-resistant–platinum-refractory ovarian cancer. *Med. Oncol.* **34**, 1–7 (2017).

79. Mistry, P., Kelland, L. R., Abel, G., Sidhar, S. & Harrap, K. R. The relationships between glutathione, glutathione-S-transferase and cytotoxicity of platinum drugs and melphalan in eight human ovarian carcinoma cell lines. *Br. J. Cancer* **64**, 215–

220 (1991).

80. Altman, B. J., Stine, Z. E. & Dang, C. V. From Krebs to clinic: glutamine metabolism to cancer therapy. *Nat. Rev. Cancer* **16**, 619–634 (2016).

81. Kamphorst, J. J. *et al.* Human pancreatic cancer tumors are nutrient poor and tumor cells actively scavenge extracellular protein. *Cancer Res.* **75**, 544–553 (2015).

82. Cluntun, A. A., Lukey, M. J., Cerione, R. A. & Locasale, J. W. Glutamine Metabolism in Cancer: Understanding the Heterogeneity. *Trends Cancer* **3**, 169–180 (2017).

83. Tardito, S. *et al.* Glutamine synthetase activity fuels nucleotide biosynthesis and supports growth of glutamine-restricted glioblastoma. *Nat. Cell Biol.* **17**, 1556–1568 (2015).

84. Ishikawa, T. & Ali-Osman, F. Glutathione-associated cis-diamminedichloroplatinum(II) metabolism and ATP-dependent efflux from leukemia cells. Molecular characterization of glutathione-platinum complex and its biological significance. *J. Biol. Chem.* **268**, 20116–20125 (1993).

85. Cairns, R. A., Harris, I. S. & Mak, T. W. Regulation of cancer cell metabolism. *Nat. Rev. Cancer* **11**, 85–95 (2011).

86. DangV., C. Links between metabolism and cancer. *Genes Dev.* **26**, 877–890 (2012).

87. Still, E. R. & Yuneva, M. O. Hopefully devoted to Q: Targeting glutamine addiction in cancer. *Br. J. Cancer* **116**, 1375–1381 (2017).

88. Hensley, C. T., Wasti, A. T. & DeBerardinis, R. J. Glutamine and cancer: cell biology, physiology, and clinical opportunities. *J. Clin. Invest.* **123**, 3678–3684 (2013).

89. Castegna, A. & Menga, A. Glutamine Synthetase: Localization Dictates Outcome. *Genes (Basel).* **19**, 9(2):108 (2018).

90. Jin, R. *et al.* Study of biological performance of Chinese materia medica with either a cold or hot property based on the three-element mathematical analysis model. *Zhong Xi Yi Jie He Xue Bao* **9**, 715–724 (2011).

91. Fu, S. *et al.* Glutamine synthetase promotes radiation resistance via facilitating nucleotide metabolism and subsequent DNA damage repair. *Cell Rep.* **28**, 1136–1143.e4 (2019).

92. Bott, A. J. *et al.* Oncogenic Myc induces expression of glutamine synthetase through promoter demethylation. *Cell Metab.* **22**, 1068–1077 (2015).

93. Furusawa, A. *et al.* Ovarian cancer therapeutic potential of glutamine depletion

based on GS expression. *Carcinogenesis* **39**, 758–766 (2018).

94. Sullivan, E. J., Kurtoglu, M., Brenneman, R., Liu, H. & Lampidis, T. J. Targeting cisplatin-resistant human tumor cells with metabolic inhibitors. *Cancer Chemother. Pharmacol.* **73**, 417–427 (2014).

95. Hudson, C. D. *et al.* Altered glutamine metabolism in platinum resistant ovarian cancer. *Oncotarget* **7**, 41637–41649 (2016).

96. Duan, G. *et al.* Increased glutamine consumption in cisplatin-resistant cells has a negative impact on cell growth. *Sci. Rep.* **8**, 8:4067 (2018).

97. Masamha, C. P. & LaFontaine, P. Molecular targeting of glutaminase sensitizes ovarian cancer cells to chemotherapy. *J. Cell. Biochem.* **119**, 6136–6145 (2018).

98. Obrist, F. *et al.* Metabolic vulnerability of cisplatin-resistant cancers. *EMBO J.* **37**, 1–15 (2018).

99. Satoh, K. *et al.* Global metabolic reprogramming of colorectal cancer occurs at adenoma stage and is induced by MYC. *Proc. Natl. Acad. Sci. U. S. A.* **114**, E7697–E7706 (2017).

100. Soga, T. *et al.* Metabolomic profiling of anionic metabolites by capillary electrophoresis mass spectrometry. *Anal. Chem.* **81**, 6165–6174 (2009).

101. Behrens, B. C. *et al.* Characterization of a cis-diamminedichloroplatinum(II)-resistant human ovarian cancer cell line and its use in evaluation of platinum analogues. *Cancer Res.* **47**, 414–418 (1987).

102. Hamilton, T. C., Young, R. C. & Ozols, R. F. Experimental model systems of ovarian cancer: applications to the design and evaluation of new treatment approaches. *Semin. Oncol.* **11**, 285–298 (1984).

103. Colanduoni, J., Nissan, R. & Villafranca, J. J. Studies of the mechanism of glutamine synthetase utilizing pH-dependent behavior in catalysis and binding. *J. Biol. Chem.* **262**, 3037–3043 (1987).

104. Conjard, A. *et al.* Inhibition of glutamine synthetase in the mouse kidney. A novel mechanism of adaptation to metabolic acidosis. *J. Biol. Chem.* **278**, 38159–38166 (2003).

105. Lu, W., Pelicano, H. & Huang, P. Cancer metabolism: is glutamine sweeter than glucose? *Cancer Cell* **18**, 199–200 (2010).

106. Kalinina, E. V., Chernov, N. N. & Novichkova, M. D. Role of glutathione, glutathione

transferase, and glutaredoxin in regulation of redox-dependent processes. *Biochem.* **79**, 1562–1583 (2014).

107. De Luca, A. *et al.* A structure-based mechanism of cisplatin resistance mediated by glutathione transferase P1-1. *Proc. Natl. Acad. Sci. U. S. A.* **116**, 13943–13951 (2019).

108. Yang, L. *et al.* Metabolic shifts toward glutamine regulate tumor growth, invasion and bioenergetics in ovarian cancer. *Mol. Syst. Biol.* **10**, 728 (2014).

109. Stäubert, C. *et al.* Rewired metabolism in drug-resistant leukemia cells: a metabolic switch hallmarked by reduced dependence on exogenous glutamine. *J. Biol. Chem.* **290**, 8348–8359 (2015).

110. Wang, L., Peng, W., Wu, T., Deng, P. & Zhao, Y.-L. Increased glutamine anabolism sensitizes non-small cell lung cancer to gefitinib treatment. *Cell Death Discov.* **4**, 84 (2018).

111. Sohn, B. H., Park, I. Y., Shin, J.-H., Yim, S. Y. & Lee, J.-S. Glutamine synthetase mediates sorafenib sensitivity in β-catenin-active hepatocellular carcinoma cells. *Exp. Mol. Med.* **50**, e421 (2018).

112. Muthu, M. *et al.* GLUL ablation can confer drug resistance to cancer cells via a malate-aspartate shuttle-mediated mechanism. *Cancers (Basel).* **11**, 1–20 (2019).

113. Bergers, G. & Fendt, S. M. The metabolism of cancer cells during metastasis. *Nat Rev Cancer.* **21**, 162–180 (2021).

114. Cruzat, V., Rogero, M. M., Keane, K. N., Curi, R. & Newsholme, P. Glutamine: Metabolism and immune function, supplementation and clinical translation. *Nutrients* **10**, 1–31 (2018).

115. Yoo, H. C., Yu, Y. C., Sung, Y. & Han, J. M. Glutamine reliance in cell metabolism. *Exp. Mol. Med.* **52**, 1496–1516 (2020).

116. Masisi, B. K. *et al.* The role of glutaminase in cancer. *Histopathology.* **76**, 498–508 (2020).

117. Yu, W. *et al.* Targeting GLS1 to cancer therapy through glutamine metabolism. *Clin. Transl. Oncol.* **23**, 2253–2268 (2021).

118. Matés, J. M., Campos-Sandoval, J. A., Santos-Jiménez, J. de los & Márquez, J. Dysregulation of glutaminase and glutamine synthetase in cancer. *Cancer Lett.* **467**, 29–39 (2019).

119. Kung, H. N., Marks, J. R. & Chi, J. T. Glutamine synthetase is a genetic determinant

of cell type-specific glutamine independence in breast epithelia. *PLoS Genet.* **7** ,e1002229 (2011).

120. Guo, J. *et al.* Reprogramming of glutamine metabolism via glutamine synthetase silencing induces cisplatin resistance in A2780 ovarian cancer cells. *BMC Cancer* **21**, 1–11 (2021).

121. Soga, T. & Heiger, D. N. Amino acid analysis by capillary electrophoresis electrospray ionization mass spectrometry. *Anal. Chem.* **72**, 1236–1241 (2000).

122. Rappsilber, J., Ishihama, Y. & Mann, M. Stop And Go Extraction tips for matrix-assisted laser desorption/ionization, nanoelectrospray, and LC/MS sample pretreatment in proteomics. *Anal. Chem.* **75**, 663–670 (2003).

123. Mun, D. G. *et al.* DIA-Based Proteome Profiling of Nasopharyngeal Swabs from COVID-19 Patients. *J. Proteome Res.* **20**, 4165–4175 (2021).

124. Meier, F. *et al.* diaPASEF: parallel accumulation–serial fragmentation combined with data-independent acquisition. *Nat. Methods* **17** ,1229–1236 (2020).

125. Okuda, S. *et al.* JPOSTrepo: An international standard data repository for proteomes. *Nucleic Acids Res.* **45**, D1107–D1111 (2017).

126. Ma, B. *et al.* PEAKS: powerful software for peptide de novo sequencing by tandem mass spectrometry. *Rapid Commun. Mass Spectrom.* **17**, 2337–2342 (2003).

127. Wang, S., Zhong, Y., Cheng, J. & Yang, H. EnrichVisBox: A Versatile and Powerful Web Toolbox for Visualizing Complex Functional Enrichment Results of Omics Data. *J. Comput. Biol.* **28**, 922–930 (2021).

128. Kanehisa, M., Sato, Y., Kawashima, M., Furumichi, M. & Tanabe, M. KEGG as a reference resource for gene and protein annotation. *Nucleic Acids Res.* **44**, D457–D462 (2016).

129. Papatheodorou, I. *et al.* Expression Atlas: Gene and protein expression across multiple studies and organisms. *Nucleic Acids Res.* **46**, D246–D251 (2018).

130. Pedreschi, R. *et al.* Treatment of missing values for multivariate statistical analysis of gel-based proteomics data. *Proteomics* **8**, 1371–1383 (2008).

131. Yang, L. *et al.* Targeting Stromal Glutamine Synthetase in Tumors Disrupts Tumor Microenvironment-Regulated Cancer Cell Growth. *Cell Metab.* **24**, 685–700 (2016).

132. Ye, J. *et al.* Targeting of glutamine transporter ASCT2 and glutamine synthetase suppresses gastric cancer cell growth. *J. Cancer Res. Clin. Oncol.* **144**, 821–833

(2018).

133. Yang, C. *et al.* Flavonoid 4,4'-dimethoxychalcone induced ferroptosis in cancer cells by synergistically activating Keap1/Nrf2/HMOX1 pathway and inhibiting FECH. *Free Radic. Biol. Med.* **188**, 14–23 (2022).

134. Gao, M. *et al.* Role of Mitochondria in Ferroptosis. *Mol. Cell* **73**, 354-363.e3 (2019).

135. Kang, R., Kroemer, G. & Tang, D. The tumor suppressor protein p53 and the ferroptosis network. *Free Radic. Biol. Med.* **133**, 162–168 (2019).

136. Wang, Y. *et al.* GLUL Promotes Cell Proliferation in Breast Cancer. *J. Cell. Biochem.* **118**, 2018–2025 (2017).

137. Fan, S. *et al.* High expression of glutamate-ammonia ligase is associated with unfavorable prognosis in patients with ovarian cancer. *J. Cell. Biochem.* **119**, 6008–6015 (2018).

138. Issaq, S. H., Mendoza, A., Fox, S. D. & Helman, L. J. Glutamine synthetase is necessary for sarcoma adaptation to glutamine deprivation and tumor growth. *Oncogenesis* **8**, 20 (2019).

139. Yang, L., Venneti, S. & Nagrath, D. Glutaminolysis: A Hallmark of Cancer Metabolism. *Annu. Rev. Biomed. Eng.* **19**, 163–194 (2017).

140. Hatem, E., El Banna, N. & Huang, M. E. Multifaceted Roles of Glutathione and Glutathione-Based Systems in Carcinogenesis and Anticancer Drug Resistance. *Antioxidants Redox Signal.* **27**, 1217–1234 (2017).

141. Ye, Y. *et al.* Repression of the antiporter SLC7A11/glutathione/glutathione peroxidase 4 axis drives ferroptosis of vascular smooth muscle cells to facilitate vascular calcification. *Kidney Int.* **102**, 1259–1275 (2022).

142. Cao, J. Y. *et al.* A Genome-wide Haploid Genetic Screen Identifies Regulators of Glutathione Abundance and Ferroptosis Sensitivity. *Cell Rep.* **26**, 1544-1556.e8 (2019).

143. Guo, J., Wang, J., Iino, K., Tomita, M. & Soga, T. Quantitative and Molecular Similarity Analyses of the Metabolites of Cold- and Hot-Natured Chinese Herbs. *Evid. Based. Complement. Alternat. Med.* **2021**, 6646507 (2021).

144. Li, M. *et al.* Integrated analysis of DNA methylation and gene expression reveals specific signaling pathways associated with platinum resistance in ovarian cancer. *BMC Med. Genomics* **2**, 34 (2009).

145. Ferreira, G. C. Ferrochelatase. *Int. J. Biochem. Cell Biol.* **31**, 995–1000 (1999).

146. Jiang, X., Stockwell, B. R. & Conrad, M. Ferroptosis: mechanisms, biology and role in disease. *Nat. Rev. Mol. Cell Biol.* **22**, 266–282 (2021).

Supplementary Materials

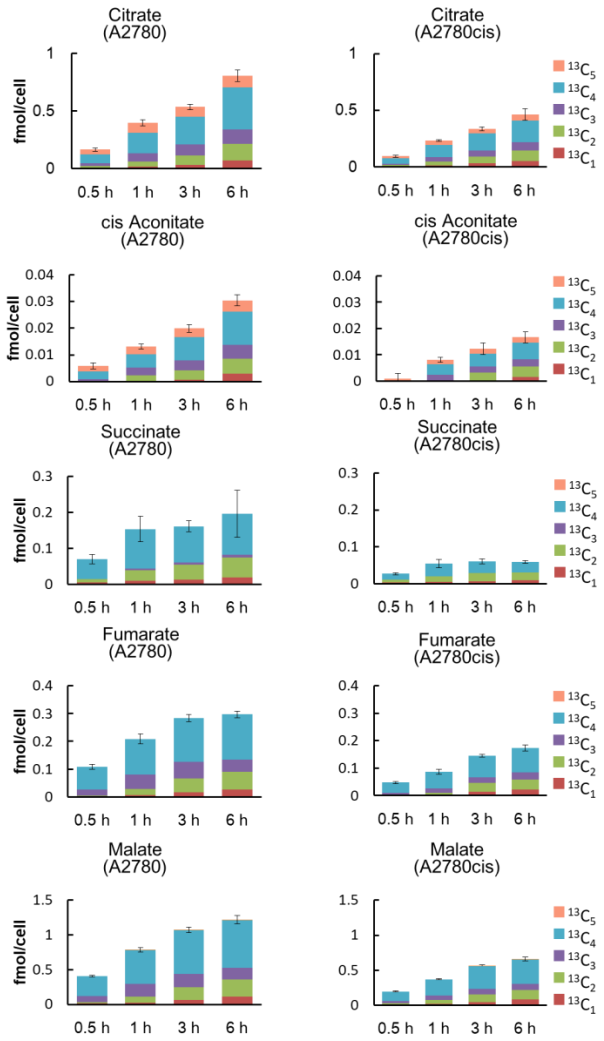

Figure S1 Metabolic flux analysis using isotopically labelled glutamine in A2780 and A2780cis cells in Chapter 3

Isotopologue distribution of metabolites in A2780 and A2780cis cells. Cells were incubation with medium containing glutamine isotopically labeled at all five carbon atoms ($^{13}C_5$-glutamine) for the indicated time periods. Carbon fluxes from glutamine to TCA cycle metabolites were determined using CE-TOF/MS. Each bar color corresponds to the number of ^{13}C replaced with ^{12}C in the metabolites. Data are shown as the mean ± SD of the three independent experiments. See also Figure 2-2.

Table S1 Primer sequences used for RT-PCR analysis in Chapter 3

GS	Forward：5‘ AGGGTTAAAGAGGGCAACCC 3’
	Reverse：5’ GAGGTGGTCATGGTGGAAGG 3’
GLUD1	Forward：5‘GGGAGGTCATCGAAGGCTAC 3’
	Reverse：5’ TCACATCAGTGCTGTAACGGA 3’
GCLC	Forward：5’ GTTCTCAAGTGGGGCGATGA 3’
	Reverse：5’ TTCTCCCCAGACAGGACCAA 3’
GSS	Forward：5’ GAACCGTTCGCGGAGGAAA 3’
	Reverse：5’ TATCCTGCAAGAGGCTCCCC 3’
GSTP1	Forward：5’ GAGGACCTCCGCTGCAAATA 3’
	Reverse：5’ CAGCAGGGTCTCAAAAGGCT 3’
β-actin	Forward：5’ CCAGCCTTCCTTCCTGGGCATGG 3’
	Reverse：5’ TTGGCGTACAGGTCTTTGCGGAT 3’
GLS	Forward：5’ TAGCTTGGAAGATTTGCTGT 3’
	Reverse：5’ CCTGTAGATTTGAGTGCTGT 3’
RPL27	Forward：5’ CTGTCGTCAATAAGGATGTCT 3’
	Reverse：5’ CTTGTTCTTGCCTGTCTTGT 3’

Table S2 Metabolites with significant differences in expression between A2780 and A2780cis cells in Chapter 3

The levels of 189 metabolites in A2780 and A2780cis cells in the presence of glutamine were determined via CE-TOF/MS using 513 metabolite standards. The levels of 50 metabolites in A2780cis cells were at least 2.0-fold higher than those in A2780 cells, whereas those of 8 metabolites were lower by 0.5-fold or less than those in A2780 cells (n=3). Statistical significance was determined using the Students' *t* test ($p<0.05$). See also Figure 3-1C.

	Fold (A2780cis/A2780)	Average (fmol/cell) (A2780)	Average (fmol/cell) (A2780cis)	p valve	
Gln	88.62	0.026	2.317	7.20E-04	Up
Glycerophosphorylcholine	13.82	0.208	2.871	1.41E-04	Up
Urea	8.92	0.447	3.993	8.41E-04	Up
Asp	8.12	0.145	1.179	2.08E-06	Up
o-Acetylcarnitine	5.69	0.233	1.328	4.56E-05	Up
Carnitine	5.52	0.007	0.038	1.52E-06	Up
Choline	5.31	0.010	0.055	2.62E-03	Up
Glycerophosphate	5.12	0.126	0.644	1.34E-03	Up
Ala	4.91	1.384	6.794	1.56E-03	Up
4-Oxopentanoate	4.83	0.037	0.180	2.06E-02	Up
GABA	4.69	0.044	0.206	3.01E-03	Up
Hypotaurine	4.54	0.142	0.647	2.68E-06	Up
beta-Ala	4.36	0.107	0.467	3.86E-04	Up
Taurine	4.31	0.391	1.686	4.26E-03	Up
Kynurenine	4.27	0.007	0.030	1.83E-03	Up
Ophthalmate	4.05	0.001	0.003	3.59E-02	Up
Creatinine	3.94	0.016	0.064	1.14E-02	Up
G1P	3.75	0.032	0.120	2.79E-03	Up
alpha-Aminoadipate	3.68	0.005	0.019	4.43E-04	Up
3-Hydroxybutyrate	3.61	0.049	0.177	2.25E-03	Up
Glu	3.37	2.953	9.962	6.15E-05	Up
Glycolate	3.31	0.070	0.233	4.41E-02	Up
Glutathione (GSH)	3.11	1.179	3.667	6.97E-05	Up
gamma-Butyrobetaine	3.09	0.009	0.027	2.55E-04	Up
threo-beta-methylaspartate	2.95	8.221	24.259	3.54E-04	Up
GDP	2.90	0.004	0.012	2.07E-02	Up

	Fold (A2780cis/A2780)	Average (fmol/cell) (A2780)	Average (fmol/cell) (A2780cis)	p valve	
Val	2.89	0.117	0.339	3.22E-03	Up
trans-Cinnamate	2.87	0.227	0.650	4.83E-03	Up
Azelate	2.84	0.009	0.026	1.81E-03	Up
Cysteine sulfinate	2.82	0.036	0.103	5.86E-03	Up
2-Hydroxybutyrate	2.77	0.016	0.045	6.85E-03	Up
Met	2.60	0.079	0.206	1.62E-06	Up
Pro	2.57	1.060	2.721	6.38E-05	Up
Nicotinamide	2.56	0.011	0.028	2.87E-04	Up
Ornithine	2.45	0.117	0.286	2.26E-03	Up
Carnosine	2.42	0.002	0.006	2.04E-02	Up
Carbamoyl phosphate	2.41	0.453	1.091	1.29E-03	Up
N-gamma-ethylglutamine	2.37	0.003	0.006	4.51E-04	Up
Thiamine	2.36	0.003	0.007	8.29E-03	Up
Betaine	2.35	0.045	0.105	1.53E-04	Up
CDP	2.29	0.006	0.013	2.46E-02	Up
Creatine	2.23	1.055	2.347	5.70E-04	Up
Leu	2.22	0.415	0.922	5.58E-05	Up
Syringate	2.20	0.077	0.169	1.13E-02	Up
Phe	2.13	0.094	0.201	3.49E-05	Up
2AB	2.11	0.021	0.045	4.23E-03	Up
Thr	2.06	0.484	0.996	8.89E-05	Up
NADP+	2.05	0.005	0.010	3.13E-02	Up
ADP	2.03	0.131	0.266	4.07E-05	Up
Lactate	2.01	11.655	23.389	2.92E-04	Up
N-Acetylputrescine	0.48	0.025	0.012	7.41E-03	Down
SAM+	0.43	0.038	0.016	1.90E-03	Down
N-Acetylglucosamine 6-phosphate	0.37	0.113	0.042	1.37E-02	Down
Argininosuccinate	0.34	0.043	0.015	1.36E-05	Down
Arg	0.28	0.819	0.231	7.33E-03	Down
Ser	0.22	0.675	0.151	2.91E-04	Down
Cystathionine	0.10	0.558	0.057	4.90E-05	Down
2-Hydroxyglutarate	0.05	0.127	0.007	1.09E-04	Down

Table S3 Metabolites with significant differences in expression between A2780 and A2780cis cells in the presence of glutamine in Chapter 3

The levels of 77 metabolites in A2780 and A2780cis cells were determined via CE-TOF/MS using 114 metabolite standards. The levels of 28 metabolites in A2780cis cells were at least 1.5-fold higher than those in A2780 cells, whereas those of 7 metabolites were lower by 0.67-fold or less than those in A2780 cells (n=3). Statistical significance was determined by Students' *t* test ($p<0.05$). See also Figure 3-3A.

	Fold (A2780cis/A2780)	Average (fmol/cell) (A2780)	Average (fmol/cell) (A2780cis)	p value	
Gln	31.67	0.139	4.400	5.26E-04	Up
Val	29.52	0.017	0.512	3.07E-05	Up
Ala	13.51	0.944	12.753	2.53E-04	Up
Asp	11.90	0.157	1.865	4.86E-04	Up
Met	11.67	0.028	0.322	4.94E-03	Up
Phe	10.40	0.029	0.303	1.84E-04	Up
F1,6P	10.23	0.052	0.530	1.33E-03	Up
Glutathione (GSH)	9.97	0.885	8.816	1.52E-04	Up
Lys	9.17	0.019	0.171	3.45E-03	Up
G6P	6.71	0.018	0.123	3.94E-03	Up
F6P	5.34	0.006	0.034	2.74E-02	Up
Glu	3.58	6.191	22.182	4.55E-05	Up
GABA	3.56	0.123	0.439	1.38E-05	Up
G1P	3.50	0.068	0.236	2.83E-03	Up
Cysteine sulfinate	3.28	0.041	0.135	2.86E-03	Up
Thr	2.97	0.535	1.589	7.54E-06	Up
CoA	2.85	0.005	0.015	1.83E-02	Up
Hypotaurine	2.56	0.666	1.705	6.26E-06	Up
Fumarate	2.55	0.073	0.185	9.49E-03	Up
ATP	2.32	1.826	4.240	4.88E-02	Up
Malate	2.30	0.307	0.707	5.18E-03	Up
DHAP	2.26	0.017	0.039	1.61E-02	Up
Pyruvate	2.18	0.346	0.755	5.88E-03	Up
Leu	2.12	0.731	1.546	3.49E-04	Up
Glycerophosphate	1.77	0.546	0.968	2.21E-02	Up
Taurine	1.67	0.440	0.737	4.37E-03	Up
Ile	1.66	0.985	1.632	2.46E-05	Up

	Fold (A2780cis/A2780)	Average (fmol/cell) (A2780)	Average (fmol/cell) (A2780cis)	p value	
PEP	1.55	0.021	0.033	1.40E-02	Up
Gly	0.58	17.570	10.164	2.18E-04	Down
Citrulline	0.55	0.127	0.070	2.44E-03	Down
Lactate	0.55	26.650	14.583	3.68E-04	Down
Ser	0.36	0.666	0.240	2.70E-04	Down
Cystathionine	0.24	0.606	0.145	3.38E-04	Down
Arg	0.20	4.333	0.882	1.65E-03	Down
2-Hydroxyglutarate	0.17	0.156	0.026	4.85E-02	Down

Table S4 Metabolites with significant differences in expression between A2780 and A2780cis cells under glutamine starvation in Chapter 3

The levels of 63 metabolites in A2780 and A2780cis cells in the absence of glutamine were determined via CE-TOF/MS using 114 metabolite standards. The levels of 10 metabolites in A2780cis cells were at least 1.5-fold higher than those in A2780 cells, whereas those of 8 metabolites were lower by 0.67-fold or less than those in A2780 cells (n=3). Statistical significance was determined by the Students' *t* test ($p<0.05$). See also Figure 3-3A.

	Fold (A2780cis/A2780)	Average (fmol/cell) (A2780)	Average (fmol/cell) (A2780cis)	p value	
Hypotaurine	9.78	0.220	2.151	1.38E-06	Up
Ala	7.93	0.417	3.306	3.64E-05	Up
Glutathione (GSH)	5.31	0.866	4.602	1.27E-02	Up
Creatine	4.98	4.520	22.521	3.13E-05	Up
Taurine	4.57	0.336	1.535	2.26E-03	Up
GABA	2.7	0.156	0.423	2.07E-04	Up
beta-Ala	2.58	0.200	0.517	2.61E-04	Up
Glycerophosphate	2.37	0.885	2.096	2.46E-02	Up
Glu	1.93	4.570	8.814	1.20E-02	Up
CDP	1.64	0.032	0.052	3.13E-02	Up
Citrulline	0.63	0.119	0.076	2.42E-02	Down
Gly	0.57	50.721	29.114	3.76E-02	Down
Tyr	0.55	1.677	0.928	4.62E-02	Down
S7P	0.34	0.164	0.056	2.74E-03	Down
Cystathionine	0.3	0.351	0.104	2.15E-02	Down
3PG	0.3	0.181	0.054	8.60E-03	Down
2-Hydroxyglutarate	0.27	0.211	0.058	3.67E-02	Down
Trp	0.23	0.362	0.083	1.73E-02	Down

Table S5 Metabolites significantly changed under glutamine starvation in A2780 cells in Chapter 3

The levels of 70 metabolites in A2780 cells in the presence (Gln+) or absence (Gln-) of glutamine were determined via CE-TOF/MS using 114 metabolite standards. The levels of 27 metabolites in the absence of glutamine were at least 1.5-fold higher than those in the presence of glutamine, whereas those of 5 metabolites were lower by 0.67-fold or less than those in the presence of glutamine (n=3). Statistical significance was determined using the Students' *t* test ($p<0.05$). See also Figure 3-3A.

	Fold (Gln-/Gln+)	Average (fmol/cell) (Gln+)	Average (fmol/cell) (Gln-)	p value	
Val	102.13	0.017	1.773	2.41E-02	Up
Lys	91.96	0.019	1.719	3.40E-02	Up
F1,6P	46.24	0.052	2.397	9.80E-03	Up
Phe	45.25	0.029	1.318	1.94E-02	Up
Met	38.60	0.028	1.064	1.77E-02	Up
DHAP	24.45	0.017	0.424	3.85E-02	Up
Ru5P	13.78	0.010	0.138	2.27E-02	Up
IMP	11.29	0.009	0.101	1.15E-02	Up
Thr	10.81	0.535	5.781	1.29E-02	Up
GTP	9.81	0.212	2.079	2.34E-02	Up
S7P	8.29	0.020	0.164	5.83E-03	Up
G1P	6.68	0.068	0.452	1.01E-03	Up
G6P	6.34	0.018	0.117	8.14E-04	Up
Ser	5.14	0.666	3.422	1.09E-02	Up
Leu	4.66	0.731	3.403	2.96E-02	Up
GDP	4.35	0.024	0.103	1.50E-02	Up
Carnosine	4.13	0.004	0.016	2.81E-02	Up
2PG	3.51	0.008	0.029	1.37E-03	Up
Tyr	3.31	0.507	1.677	2.25E-02	Up
3PG	3.13	0.058	0.181	2.00E-02	Up
PEP	2.89	0.021	0.062	1.77E-04	Up
Gly	2.89	17.570	50.721	1.75E-02	Up
dTTP	2.70	0.018	0.047	7.76E-03	Up
SAM+	2.28	0.019	0.044	1.05E-03	Up
ADP	2.27	0.257	0.585	3.77E-02	Up

	Fold (Gln-/Gln+)	Average (fmol/cell) (Gln+)	Average (fmol/cell) (Gln-)	p value	
AMP	2.23	0.053	0.119	9.58E-05	Up
Asn	2.21	6.985	15.414	2.96E-02	Up
Cystathionine	0.58	0.606	0.351	2.48E-02	Down
Taurine	0.56	0.440	0.247	3.13E-03	Down
Ala	0.44	0.944	0.417	2.36E-02	Down
Hypotaurine	0.33	0.666	0.220	2.36E-04	Down
beta-Ala	0.28	0.716	0.200	1.18E-04	Down

Table S6 Metabolites significantly changed under glutamine starvation in A2780cis cells in Chapter 3

The levels of 63 metabolites in A2780cis cells in the presence (Gln+) or absence (Gln-) of glutamine were determined via CE-TOF/MS using 114 metabolite standards. The levels of 23 metabolites in the absence of glutamine were at least 1.5-fold higher than those in the presence of glutamine, whereas those of 9 metabolites were lower by 0.67-fold or less than those in the presence of glutamine (n=3). Statistical significance was determined using the Students' *t* test ($p<0.05$). See also Figure 3-3A.

	Fold (Gln-/Gln+)	Average (fmol/cell) (Gln+)	Average (fmol/cell) (Gln-)	p value	
Ser	17.25	0.240	4.138	7.52E-04	Up
Creatine	5.32	4.233	22.521	8.09E-04	Up
Lys	3.87	0.171	0.663	1.08E-02	Up
F1,6P	3.81	0.530	2.021	1.96E-05	Up
CDP	3.01	0.017	0.052	1.67E-02	Up
Gly	2.86	10.164	29.114	9.24E-04	Up
Arg	2.65	0.882	2.336	6.13E-03	Up
GDP	2.64	0.051	0.135	2.48E-03	Up
Thr	2.58	1.589	4.103	5.16E-04	Up
Phe	2.33	0.303	0.705	1.00E-02	Up
AMP	2.30	0.057	0.130	9.65E-05	Up
Glycerophosphate	2.16	0.968	2.096	3.10E-02	Up
Val	2.15	0.512	1.103	8.71E-03	Up
Taurine	2.08	0.737	1.535	2.15E-02	Up
2-Hydroxyglutarate	2.05	0.026	0.054	9.45E-03	Up
ADP	2.02	0.366	0.741	5.52E-05	Up
Met	1.95	0.322	0.629	7.68E-04	Up
SAM+	1.74	0.024	0.043	1.04E-03	Up
Tyr	1.73	0.537	0.928	7.36E-03	Up
Glutathione (GSSG)	1.66	1.217	2.024	1.47E-02	Up
Asn	1.57	6.229	9.782	3.35E-03	Up
CTP	1.57	0.296	0.465	1.92E-02	Up
G1P	1.56	0.236	0.369	8.60E-03	Up
Citrate	0.66	1.035	0.680	3.87E-02	Down
beta-Ala	0.53	0.981	0.517	6.24E-05	Down
Glutathione (GSH)	0.52	8.816	4.602	2.21E-03	Down
cis-Aconitate	0.51	0.051	0.026	2.43E-02	Down
Fumarate	0.43	0.185	0.079	1.16E-02	Down
Malate	0.41	0.707	0.292	2.25E-04	Down
Glu	0.40	22.182	8.814	2.17E-04	Down

	Fold (Gln-/Gln+)	Average (fmol/cell) (Gln+)	Average (fmol/cell) (Gln-)	p value	
Asp	0.27	1.865	0.495	2.10E-05	Down
Ala	0.26	12.753	3.306	9.46E-05	Down

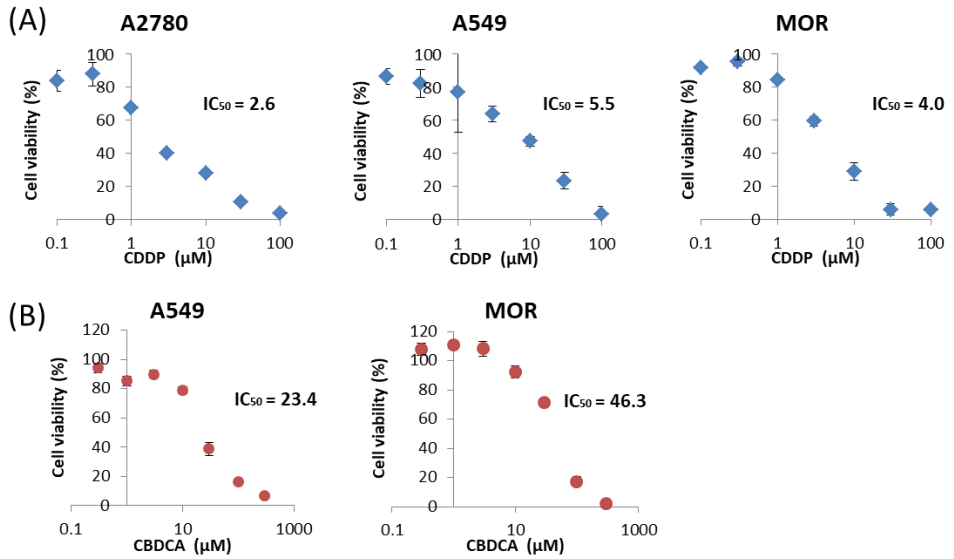

Figure S2 Evaluate CDDP and CBDCA sensitivity in the cancer cell lines in Chapter 4

(A) Effects of CDDP exposure after 48 h on cell viability of A2780, A549, and MOR cells, and cell viability was evaluated by MTT assay. The cell doubling time of A2780 was faster than that of A549 and MOR, so the seeding number of A2780 was 4000 cells, and that of A549 and MOR was 8000 cells. The IC50 of A2780, A549 and MOR were 2.6 μM, 5.5 μM and 4.0 μM CDDP, respectively. (B) Effects of CBDCA exposure after 72 h on cell viability of A549 and MOR cells, and cell viability was measured by MTT assay. The IC50 of A549 and MOR was 23.4 μM and 46.3 μM CBDCA, respectively.

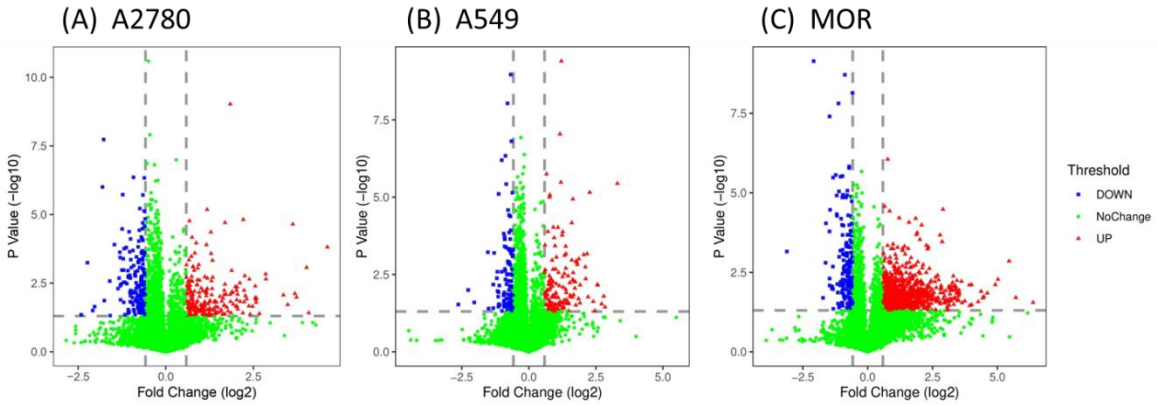

Figure S3 Differential expression analysis of three cell lines in Chapter 4

(A, B, C) Volcano plot showing all quantified proteins distributed by fold change and p-value in a log scale (shGLUL over NT). The dashed lines represent the significance thresholds. Red triangles represent upregulated proteins and blue squares represent downregulated proteins.

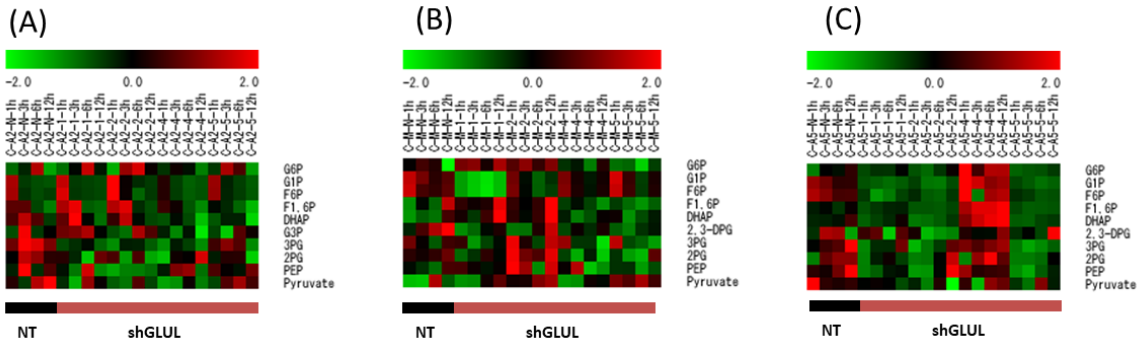

Figure S4 Heatmap is based on the compounds in the glycolysis pathway from three cell lines in Chapter 4

(A, B, C) Rows represent compounds, and the ordinates represent cell samples. A, B, and C are A2780, MOR, and A549 cells, respectively. The black box groups negative control cells, and the red box groups shGLUL cell lines. The color key indicates the relative concentration of the compound being determined: red, black, and green indicate high, intermediate, and low concentrations, respectively.